

TDE 2025abcr: A Tidal Disruption Event in the Outskirts of a Massive Galaxy

ROBERT STEIN ,^{1,2,3,*} JONATHAN CARNEY ,⁴ CHARLOTTE WARD ,⁵ RAFFAELLA MARGUTTI ,^{6,7,8}
 XANDER J. HALL ,⁹ ITAI SFARADI ,^{6,8} IGOR ANDREONI ,⁴ RYAN CHORNOCK ,^{6,8} SUVI GEZARI ,¹
 GEOFFREY MO ,^{10,11} YUHAN YAO ,^{12,6,8} ERIC C. BELLM ,¹³ JOSHUA S. BLOOM ,⁶ MALTE BUSMANN ,^{14,15}
 ILARIA CAIAZZO ,¹⁶ S. BRADLEY CENKO ,^{3,2} MATTHEW J. GRAHAM ,¹⁰ STEVEN L. GROOM ,¹⁷
 DANIEL GRUEN ,^{14,15} ERICA HAMMERSTEIN ,^{6,8} MANSI M. KASLIWAL ,¹⁰ BRENDAN O'CONNOR ,⁹
 ANTONELLA PALMESE ,⁹ JOSIAH PURDUM ,¹⁸ JILLIAN C. RASTINEJAD ,^{1,†} REED RIDDLE ,¹⁸ BEN RUSHOLME ,¹⁷
 JESPER SOLLERMAN ,¹⁹ JEAN J. SOMALWAR ,^{6,20} AND SYLVAIN VEILLEUX ,^{1,2}

¹ Department of Astronomy, University of Maryland, College Park, MD 20742, USA

² Joint Space-Science Institute, University of Maryland, College Park, MD 20742, USA

³ Astrophysics Science Division, NASA Goddard Space Flight Center, Mail Code 661, Greenbelt, MD 20771, USA

⁴ Department of Physics and Astronomy, University of North Carolina at Chapel Hill, Chapel Hill, NC 27599-3255, USA

⁵ Department of Astronomy & Astrophysics, 525 Davey Lab, 251 Pollock Road, The Pennsylvania State University, University Park, PA 16802, USA

⁶ Department of Astronomy, University of California, Berkeley, CA 94720-3411, USA

⁷ Department of Physics, University of California, Berkeley, CA 94720-7300, USA

⁸ Berkeley Center for Multi-messenger Research on Astrophysical Transients and Outreach (Multi-RAPTOR), University of California, Berkeley, CA 94720-3411, USA

⁹ McWilliams Center for Cosmology and Astrophysics, Department of Physics, Carnegie Mellon University, 5000 Forbes Avenue, Pittsburgh, PA 15213

¹⁰ Division of Physics, Mathematics and Astronomy, California Institute of Technology, Pasadena, CA 91125, USA

¹¹ The Observatories of the Carnegie Institution for Science, Pasadena, CA 91101, USA

¹² Miller Institute for Basic Research in Science, 206B Stanley Hall, Berkeley, CA 94720, USA

¹³ DIRAC Institute, Department of Astronomy, University of Washington, 3910 15th Avenue NE, Seattle, WA 98195, USA

¹⁴ University Observatory, Faculty of Physics, Ludwig-Maximilians-Universität München, Scheinerstr. 1, 81679 Munich, Germany

¹⁵ Excellence Cluster ORIGINS, Boltzmannstr. 2, 85748 Garching, Germany

¹⁶ Institute of Science and Technology Austria, Am Campus 1, 3400 Klosterneuburg, Austria

¹⁷ IPAC, California Institute of Technology, 1200 E. California Blvd, Pasadena, CA 91125, USA

¹⁸ Caltech Optical Observatories, California Institute of Technology, Pasadena, CA 91125, USA

¹⁹ The Oskar Klein Centre, Department of Astronomy, Stockholm University, AlbaNova, SE-10691 Stockholm, Sweden

²⁰ Kavli Institute for Particle Astrophysics and Cosmology, Stanford, CA 94305, USA

ABSTRACT

Tidal disruption events (TDEs) have traditionally been discovered in optical sky surveys through targeted searches of nuclear transients. However, it is expected that some TDEs will occur outside the galaxy nucleus, arising from wandering black holes originating in galaxy mergers. Here we present observations of TDE 2025abcr, the first optical TDE discovered in the outskirts of a host galaxy. The TDE was identified by a custom ‘off-nuclear’ implementation of the ML classifier `tdescore`, which classifies new ZTF transients based on their lightcurves. Follow-up observations confirm that TDE 2025abcr is a TDE-H+He, occurring 9.5” (10.3 kpc projected distance) from the nucleus of a massive galaxy ($M_\star = 10^{11.18 \pm 0.03} M_\odot$) with a central black hole mass of $10^{8.82 \pm 0.65} M_\odot$. TDE 2025abcr itself was likely disrupted by a much lighter black hole ($10^{6.09 \pm 0.53} M_\odot$, as estimated with peak luminosity scaling relations). The black hole was either dynamically ejected from the nucleus or lies at the center of a very faint tidally-stripped dwarf galaxy undergoing a minor merger. Late-time observations of TDE 2025abcr could confirm the origin of this apparent ‘orphan’ black hole. The rate of highly offset ($\gtrsim 3$ kpc) TDEs can be constrained to $< 10\%$ of the nuclear TDE rate, but our discovery implies that many dozens of similar sources will be detected by the Vera C. Rubin each year with resolvable offsets.

Keywords: Transient sources (1851) — Supermassive black holes (1663) — Sky Surveys (1464) — Time domain astronomy (2109)

1. INTRODUCTION

Tidal disruption events (TDEs) occur when stars pass close to massive black holes (BHs) (M. J. Rees 1988), generating a luminous flare that is detectable across the electromagnetic spectrum (see S. Gezari 2021, for a review). They offer a unique probe of otherwise-quiescent BHs, providing a window into BH demographics, and accretion physics. While the first candidate TDEs were identified via X-ray emission, the bulk of the ~ 200 known TDEs (see e.g. N. Franz et al. 2025, for a recent compilation) are now found via time-domain optical surveys such as the Zwicky Transient Facility (ZTF; E. C. Bellm et al. 2019; M. J. Graham et al. 2019; R. Dekany et al. 2020). It is widely accepted that massive BHs lie at the heart of most if not all galaxies (J. Kormendy & L. C. Ho 2013), and searches for TDEs have therefore been naturally focussed on studying ‘nuclear’ transients (e.g. S. van Velzen et al. 2011; T. Hung et al. 2018; S. van Velzen et al. 2021; E. Hammerstein et al. 2023; Y. Yao et al. 2023; Y. Dgany et al. 2023; M. Masterson et al. 2024; J. J. Somalwar et al. 2025a; I. Grotova et al. 2025; Z. Zhang et al. 2025). However, given that mergers are thought to contribute substantially to the growth of galaxies, a single galaxy could host many additional massive BHs. A smoking-gun signature for these additional BHs would therefore be the detection of a TDE with a significant offset from the center of a galaxy (see e.g. A. Ricarte et al. 2021a).

Several off-nuclear TDEs have now been found. The earliest candidate was WINGS J134849.88+263557.5 (W. P. Maksym et al. 2013, 2014), discovered via its X-ray emission, with a faint detected underlying host ($M_V = -14.8$) that is a likely dwarf galaxy. More recently, 3XMM J2150 was identified via its X-ray emission (D. Lin et al. 2020) and was located in a faint extended source thought to be a globular cluster or ultracompact dwarf galaxy. Another X-ray selected TDE candidate is EP240222A / AT 2024agqv (C. C. Jin et al. 2025), identified by the Einstein Probe (EP; W. Yuan et al. 2022). This TDE had a very faint transient optical counterpart ($M_g = -14.6$), and was also located in a tiny satellite galaxy offset 35 kpc from a large neighbouring galaxy at the same redshift (C. C. Jin et al. 2025). Amongst the recent sample of 31 X-ray selected

TDEs from eROSITA (I. Grotova et al. 2025), one source (eRASS J142140.3-295325) was located in a merging system offset 18" (21 kpc) and 24" (28 kpc) from the centers of two galaxies with an accompanying faint optical flare. Another recent candidate is HLX-1 in NGC 6099, a X-ray selected candidate intermediate-mass black hole (IMBH)-TDE (Y.-C. Chang et al. 2025).

There has also been one confirmed optically-selected source: off-nuclear TDE 2024tvd (Y. Yao et al. 2025). This TDE was discovered by ZTF (J. Sollerman et al. 2024) and initially classified as a classical TDE owing to its roughly nuclear location (S. Faris et al. 2024). However, multi-wavelength observations at high spatial resolution confirm that the TDE itself is located 0.9" (0.8 kpc) from the center of its host galaxy (Y. Yao et al. 2025). Replicating this discovery remains challenging, because similar offsets could only be resolved for TDEs occurring in nearby galaxies, and they require expensive follow-up for confirmation. A more recent candidate was AT 2024puz, an exceptional rapid transient of uncertain origin that was discovered in a search for constant-colour off-nuclear ZTF transients (J. J. Somalwar et al. 2025b). The source exhibited properties lying between those of a luminous fast blue optical transient and a TDE, in contrast to TDE 2024tvd which clearly resembled a ‘classical’ optical TDE in all respects.

The ZTF collaboration recently began a new search for off-nuclear TDEs at any projected offset, adapting the existing realtime scanning infrastructure built around the machine-learning classifier `tdescore` (R. Stein et al. 2024, in prep.). We here present the first off-nuclear TDE identified by this search: TDE 2025abcr. The source was identified as a candidate TDE by `tdescore` based on its lightcurve properties, and subsequent follow-up data confirms this classification. The source exhibits luminous UV and soft X-ray emission, as expected for a TDE, and spectroscopic observations also match known TDEs.

The paper is organised as follows: Section 2 outlines the real-time search for off-nuclear TDEs, while Section 3 outlines the multi-wavelength observations of TDE 2025abcr. Section 4 outlines the data analysis and modeling of the transient and host, while Section 5 considers the possible origin of the parent BH. Finally, we summarise our results and provide an outlook in Section 6. Throughout the paper, we assume a flat Λ CDM cosmology with $h = 0.7$, $\Omega_M = 0.3$ and $\Omega_\Lambda = 0.7$.

* Neil Gehrels Prize Postdoctoral Fellow

† NHFP Einstein Fellow

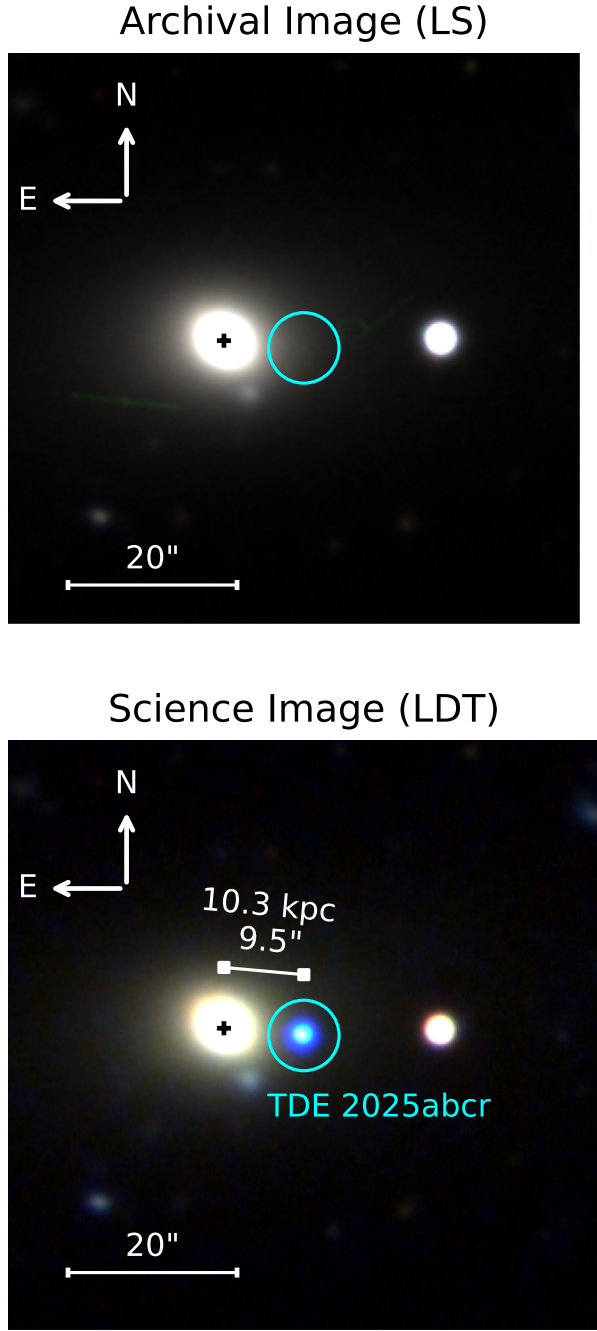


Figure 1. **Top:** Archival composite g/r/i image from Legacy Survey DR10, with the position of the transient (blue circle) and host galaxy (marked with the black + symbol). No source is visible at the transient position to a depth of 23.78 mag (see Section 4.2.2 for more details), ruling out the possibility of a bright dwarf galaxy origin for TDE 2025abcr. **Bottom:** Composite u/g/i image of TDE 2025abcr, taken with LDT on 2025-12-14. The transient (circled in blue) is significantly offset (9.5'' / 10.3 kpc) from the center of the host galaxy WISEA J014656.04-152214.7.

2. DISCOVERY WITH `tdescore`

While historical searches for optical TDEs have relied on simple algorithmic cuts (see e.g. S. van Velzen et al. 2021; E. Hammerstein et al. 2023; Y. Yao et al. 2023), dedicated machine-learning classifiers have proliferated in recent years (S. Gomez et al. 2023; R. Stein et al. 2024; X. Sheng et al. 2024; M. Pavez-Herrera et al. 2025; M. Llamas Lanza et al. 2025; K. Bhardwaj et al. 2025; R. Zheng et al. 2025). Within ZTF, the classifier `tdescore` (R. Stein et al. 2024) is now the primary means of identifying new TDEs. The classifier is a simple binary classifier, which combines high-level lightcurve properties (e.g. rise time, color at peak) with host galaxy properties (e.g. WISE $W1 - W2$ color) and transient detection properties (e.g. average offset from host galaxy). Following the implementation of a real-time `tdescore` ranking framework in July 2024 (R. Stein et al. in prep.), the majority of new optical TDEs have been identified by `tdescore`.

Since July 2025, the realtime `tdescore` framework has been expanded to encompass more agnostic searches for new TDEs. Two new versions of `tdescore` were developed: an unbiased classifier which uses lightcurve features and nuclearity but no specific information about the host itself, and a completely agnostic ‘off-nuclear’ classifier that relies exclusively on transient lightcurve properties without any knowledge about a possible host. The latter classifier runs on every new ZTF transient, and is intended to capture ‘non-nuclear’ TDEs which are either offset from a galaxy or have a host which is too faint to be recovered in the reference Pan-STARRS1 (PS1; K. C. Chambers et al. 2016) catalogue.

The implementation of a classifier agnostic to nuclearity presents additional classification and computational challenges. TDEs represent a tiny fraction ($\sim 2\%$) of nuclear sources, being outnumbered by supernovae (SNe) and active galactic nucleus (AGN) flares. Even after removing all variables, TDEs represent only $\sim 8\%$ of all nuclear transients (R. Stein et al. 2024). When broadening a search to encompass all transients, the contaminant rate increases even further. Most SNe have a significant offset from the host galaxy nucleus (see e.g. L. Wang et al. 1997), and within a flux-limited survey TDEs represent just $\sim 0.5\%$ of all transients (D. A. Perley et al. 2020). Nonetheless, `tdescore` is able to identify TDEs with relatively high precision. Since the implementation of real-time ranking, several known nuclear TDEs were recovered by the off-nuclear `tdescore` classifier with a high score (for example TDE 2025vjq (P. Charalampopoulos 2025a,b), TDE 2025aarm (M. Newsome et al. 2025; S. Faris et al. 2025) and TDE 2025aljd (R. Chornock et al. 2026a,b)).

TDE 2025abcr was first selected as a candidate TDE by the ‘off-nuclear’ `tdescore` on 2025-11-04, and assigned for spectroscopic follow-up. In this case, the ML classification by `tdescore` was driven primarily by the high lower bound on blackbody temperature ($T > 10^{4.02}$ K), the poor fit to a Type Ia SN with `sncosmo` (K. Barbary et al. 2016) (χ^2 per d.o.f. = 4.5), and the best-fit temperature increasing with time rather than cooling (+87 K per day). A waterfall plot explaining the reasoning behind the `tdescore` classification is shown in Appendix Figure 9, while the full `tdescore` source page for TDE 2025abcr is shown in Appendix Figure 10.

Subsequent multi-wavelength follow-up observations confirmed that the source was indeed a TDE, with the source exhibiting the unique spectroscopic signatures, UV emission and transient soft X-ray emission which distinguish TDEs from SNe and other contaminants. The classification was promptly reported to the community via a TNS classification (R. Stein et al. 2025a) and astronote (R. Stein et al. 2025b).

TDE 2025abcr was notable because it was significantly offset (9.5"/10.3 kpc projected distance) from the center of its apparent host (see Figure 1), located in the outskirts of a massive galaxy of known redshift. For this reason, TDE 2025abcr was not identified by any other ongoing TDE search effort. This is the first TDE found by the ‘off-nuclear’ `tdescore` that was not also identified by the ‘classic’ or ‘unbiased’ selections.

3. OBSERVATIONS OF TDE 2025abcr

We here outline the various observations of TDE 2025abcr. Photometric observations are summarised in Figure 2, and listed in Appendix Table 2. Spectroscopic observations are presented in Figure 3 and listed in Appendix Table 3. The follow-up was coordinated and data uploaded through the `fritz.science` instance of `Skyportal` (S. J. van der Walt et al. 2019; M. W. Coughlin et al. 2023).

3.1. Optical Observations

On 2025-10-13, ZTF first detected a new optical transient, assigned the internal name ZTF25abxvhmk, in the footprint of the Northern-sky public survey. The source was reported to TNS as a transient on 2025-10-21, and assigned the designation AT 2025abcr (J. Sollerman et al. 2025). Observations were processed by the standard ZTF data reduction pipeline (F. J. Masci et al. 2019), and additional detections were recovered with the ZTF alert forced photometry²¹. The source was

detected in both g –band and r –band with an exceptionally blue color ($g - r = -0.3$ mag). TDE 2025abcr brightened over a period of four weeks to a g –band on 2025-11-14 (see Figure 2), and has since been slowly fading.

The source was also imaged in the optical with the Large Monolithic Imager (LMI) of the 4.3m Lowell Discovery Telescope (LDT; S. E. Levine et al. 2012, PI: Stein) on 2024-12-14. Images were reduced using the LMI pipeline built with `mirar` (R. D. Stein et al. 2025), using Gaia DR3 (Gaia Collaboration 2021) for astrometric calibration. Photometric calibration was performed using PanSTARRS (PS1; K. C. Chambers et al. 2016) for $g/r/i$ and SkyMapper (C. A. Onken et al. 2024) for u –band. A composite cutout of the $u/g/i$ images is shown in Figure 1.

3.2. UV observations

Observations of TDE 2025abcr were requested with the *Neil Gehrels Swift Observatory* (N. Gehrels et al. 2004) for multiple epochs, beginning 5 days before peak. Imaging was conducted with the Ultra-Violet/Optical Telescope (UVOT; P. W. A. Roming et al. 2005) in all UV filters (u /UVW1/UVM2/UVW2). The UVOT observations were downloaded and reduced using `uvotredux`²² (R. D. Stein & J. Carney 2025), a Dockerized open-source python package for automated UVOT data reduction using `swifttools`²³ and `HEASoft`²⁴. Photometry was extracted assuming a 5" aperture centred on the position of the transient, with an offset 10" aperture to estimate the background. These observations revealed a bright source at the position of TDE 2025abcr, separated from the nearby host galaxy nucleus.

3.3. NIR Observations

We observed TDE 2025abcr in the near infrared (NIR) with the Three Channel Imager (3KK; F. Lang-Bardl et al. 2016) instrument mounted on the 2.1 m Fraunhofer Telescope at Wendelstein Observatory (U. Hopp et al. 2014) in the J and K_s bands. The CMOS data were reduced using a custom pipeline (C. A. Gössl & A. Riffeser 2002; M. Busmann et al. 2025). Astrometric calibration of the images was performed using the Gaia EDR3 catalog (Gaia Collaboration 2021; L. Lindegren et al. 2021; Gaia Collaboration 2020). Tools from the AstrOmatic software suite (E. Bertin & S. Arnouts 1996; E. Bertin 2006; E. Bertin et al. 2002) were used for the

²¹ <https://zwickytransientfacility.github.io/ztf-avro-alert/schema.html>

²² <https://github.com/robertdstein/uvotredux>

²³ <https://github.com/Swift-SOT/swifttools>

²⁴ <https://heasarc.gsfc.nasa.gov/docs/software/lheasoft/>

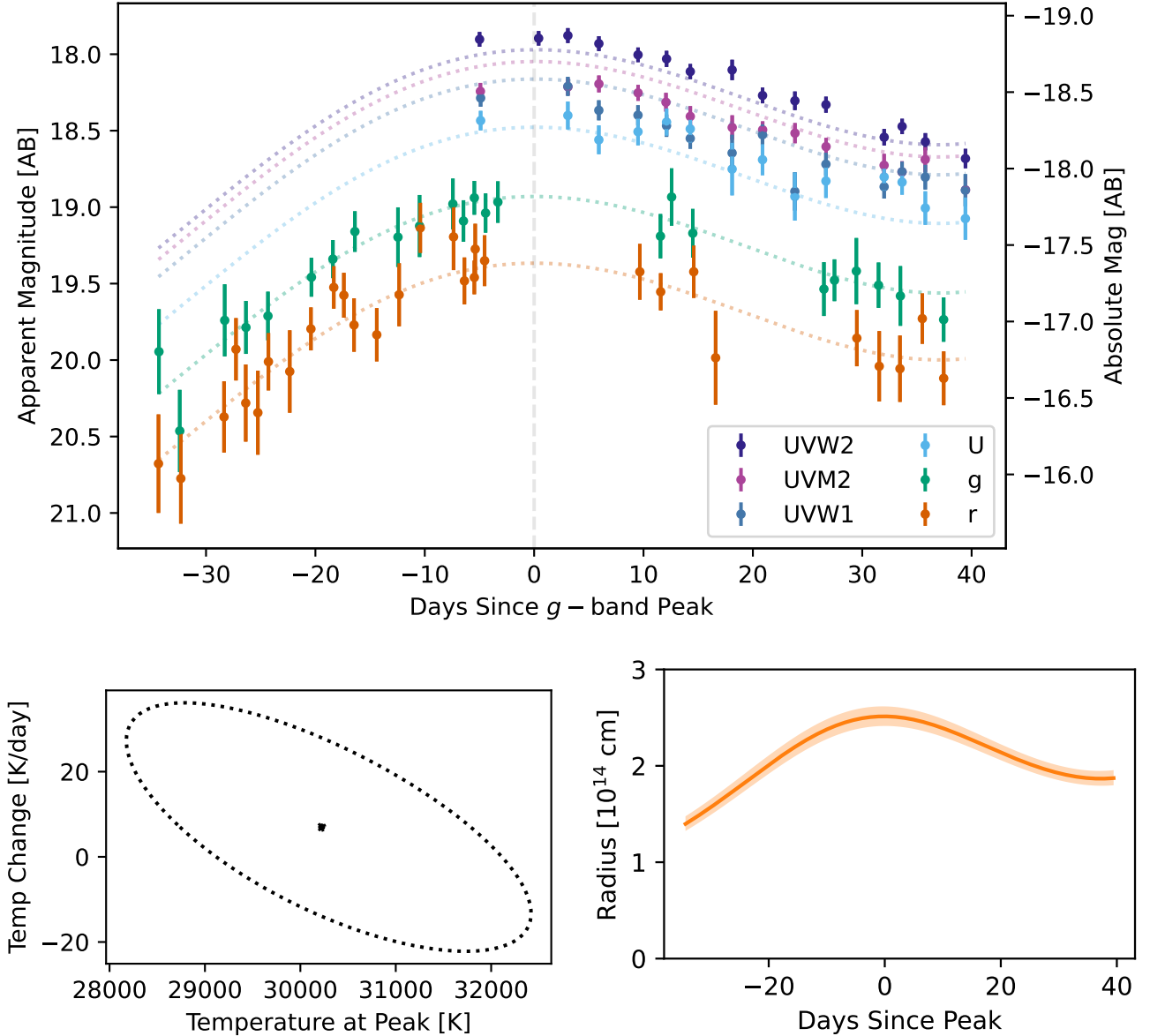


Figure 2. **Top:** Extinction-corrected UV/optical/NIR lightcurve of TDE 2025abcr, alongside a blackbody fit to the data described in Section 4.1.1. The lightcurve is well described by a single black body with a linearly-evolving temperature. **Lower Left:** 1σ uncertainty contour for the best-fit peak temperature and cooling rate. The temperature appears to change very little over time. **Lower Right:** Inferred blackbody radius as a function of time. The shaded region corresponds to the envelope of inferred radii when sampling the 1σ peak temperature/cooling ellipse.

coaddition of each epoch’s individual exposures. We calibrate against the 2MASS Catalog (M. F. Skrutskie et al. 2006). We use templates from Visible and Infrared Survey Telescope for Astronomy (VISTA; N. J. G. Cross et al. 2012) and the Saccadic Fast Fourier Transform (SFFT; L. Hu et al. 2022) algorithm for image subtraction. The source was not significantly detected ($>3\sigma$) in any of these observations, so we provide upper limits in Appendix Table 2.

3.4. High-Cadence Imaging

We observed TDE 2025abcr with the prototype *Cerberus* high-speed imager mounted at the prime focus of the 200-inch Hale telescope at Palomar Observatory (G. Mo et al. in prep.), to search for any evidence of rapid variability. The observations were performed on 2025-11-24, lasting 10 min in the SDSS- g band at 1 s cadence and 10 min in the SDSS- u band at 5 s cadence. The data were reduced with a custom pipeline (G. Mo et al. in prep.). We detect TDE 2025abcr clearly in individual

exposures, with signal-to-noise (S/N) ratios of ≈ 30 in g and ≈ 8 in u . Using a Lomb-Scargle periodogram (N. R. Lomb 1976; J. D. Scargle 1982), we find no significant evidence for periodic behaviour, with no peak exceeding the 1% false alarm probability threshold.

3.5. Spectroscopic Observation

3.5.1. Optical Spectroscopy of TDE 2025abcr

The first spectrum of TDE 2025abcr was taken with the low-resolution P60/SED Machine (SEDm; N. Blagorodnova et al. 2018) on 2025-11-05 (PI: Stein), and reduced using the standard `pysedm` pipeline (M. Rigault et al. 2019; Y.-L. Kim et al. 2022). The spectrum revealed a blue continuum with no obvious SN features, but the resolution was insufficient for a classification. Simultaneous photometry was derived through the automated pipeline, and is listed in Appendix Table 2.

Additional spectra were obtained with the Goodman High Throughput Spectrograph (GHTS; J. C. Clemens et al. 2004) mounted on the 4.1 m Southern Astrophysical Research (SOAR) telescope on 2025-11-08 and 2025-11-30 (PI: Carney). These were reduced using the standard GHTS pipeline with `pypeit` (J. X. Prochaska et al. 2020a,b). An additional SOAR epoch was taken on 2025-11-14 (PI: Clemens) and reduced using the custom Python routine outlined in B. C. Kaiser et al. (2021).

A spectrum was taken using the Low-Resolution Imaging Spectrometer (LRIS; J. B. Oke et al. 1995) on the 10 m Keck-I telescope on 2025-11-21 (PI: Chornock). A spectrum was also taken using the Kast Double Spectrograph (Kast; J. Miller & R. Stone 1993) on the 3 m Shane Telescope on 2025-11-26 (PI: Chornock). Poor conditions during both the LRIS and Kast observations resulted in exposures with substantially varying signal-to-noise ratios that required flux normalization and weighting by the inverse variance before coaddition. Both the LRIS and Kast data were reduced following standard procedures outlined by J. M. Silverman et al. (2012). An additional spectrum was taken with the DeVeney spectrograph on LDT on 2025-12-14 (PI: Stein). The data were reduced using the DeVeney pipeline in `PypeIt` (J. X. Prochaska et al. 2020a,b).

These spectra are shown in Figure 3. They confirm that the source had a blue continuum, with broad H and He emission lines at a consistent redshift of $z = 0.05$. The spectral shape and features confirm the classification of TDE 2025abcr as a tidal disruption event, and that it falls into the TDE-H+He subclass following the nomenclature introduced in S. van Velzen et al. (2021). The temporal evolution of key lines is shown in greater detail in Appendix Figure 7, and a summary of all observations is provided in Appendix Table 3.

3.5.2. Host Galaxy Spectra

A spectrum host WISEA J014656.04-152214.7 was obtained using SOAR on 2025-12-08 (PI: Carney), and was also reduced with the same `pypeit` routine as the transient spectra. The spectrum is shown in Appendix Figure 8. The host galaxy does not display any of the classic AGN signatures (Balmer lines, [O III] at $\lambda 4959 / \lambda 5007$). However, there are several clear absorption features: Ca II at $\lambda 3934 / \lambda 3969$ and Na I ($\lambda 5890 / \lambda 5896$) consistent with the archival 6dF redshift of $z = 0.049848 \pm 0.00015$ (D. H. Jones et al. 2009).

3.6. X-ray observations

We started observing TDE 2025abcr with the X-Ray Telescope (XRT; D. N. Burrows et al. 2005) on board the *Neil Gehrels Swift Observatory* (N. Gehrels et al. 2004) on 2025-11-09T14:49:31 ($\delta t = -4.82$ d, PI: X. Hall). Here we present the analysis of the XRT observations acquired until 2025-12-11T10:32:54 ($\delta t = 25.48$ d, PIs Stein, Guo; total exposure of 23.8 ks). The observations are shown in Figure 4, and listed in Appendix Table 4.

We processed the XRT data with HEASoft v6.36 and corresponding calibration files. An X-ray source is blindly detected at a position consistent with the optical transient in the first segment of observations at $\delta t = -4.82$ d with count-rate $\approx 2 \times 10^{-2}$ cts s $^{-1}$, significance of 4.5σ Gaussian equivalent. The source is not blindly detected in individual observation segments at $\delta t > -4.6$ d, implying very rapid fading of the X-ray emission and the physical association of the X-ray source with TDE 2025abcr.

Performing a targeted detection at the location of the X-ray transient following P. A. Evans et al. (2009); R. Margutti et al. (2013) leads to the recovery of a very faint X-ray source that persists until the end of our monitoring. By extracting the light-curves in two sub-energy bands (i.e., 0.3–1 keV vs. 1–10 keV), we find that the temporal evolution of the X-ray source is connected with the rapid fading of the very soft X-ray emission below the threshold of detectability for XRT, while the harder X-rays are consistent with a constant emission throughout the entire duration of our observations. With the angular resolution of the XRT we cannot rule out a dominant contribution of the host-galaxy emission to the harder X-rays.

We extracted a spectrum using data taken between 2025-11-09T14:48:59.347 and 2025-11-09T23:01:48.401 (exposure of 2.9 ks). The spectrum is dominated by very soft X-ray emission. We fit the spectrum with an absorbed multitemperature disk spectrum (i.e., `tbabs*zashift*ezdiskbb` within `Xspec`). We employ W-statistics and use MCMC analysis to estimate the

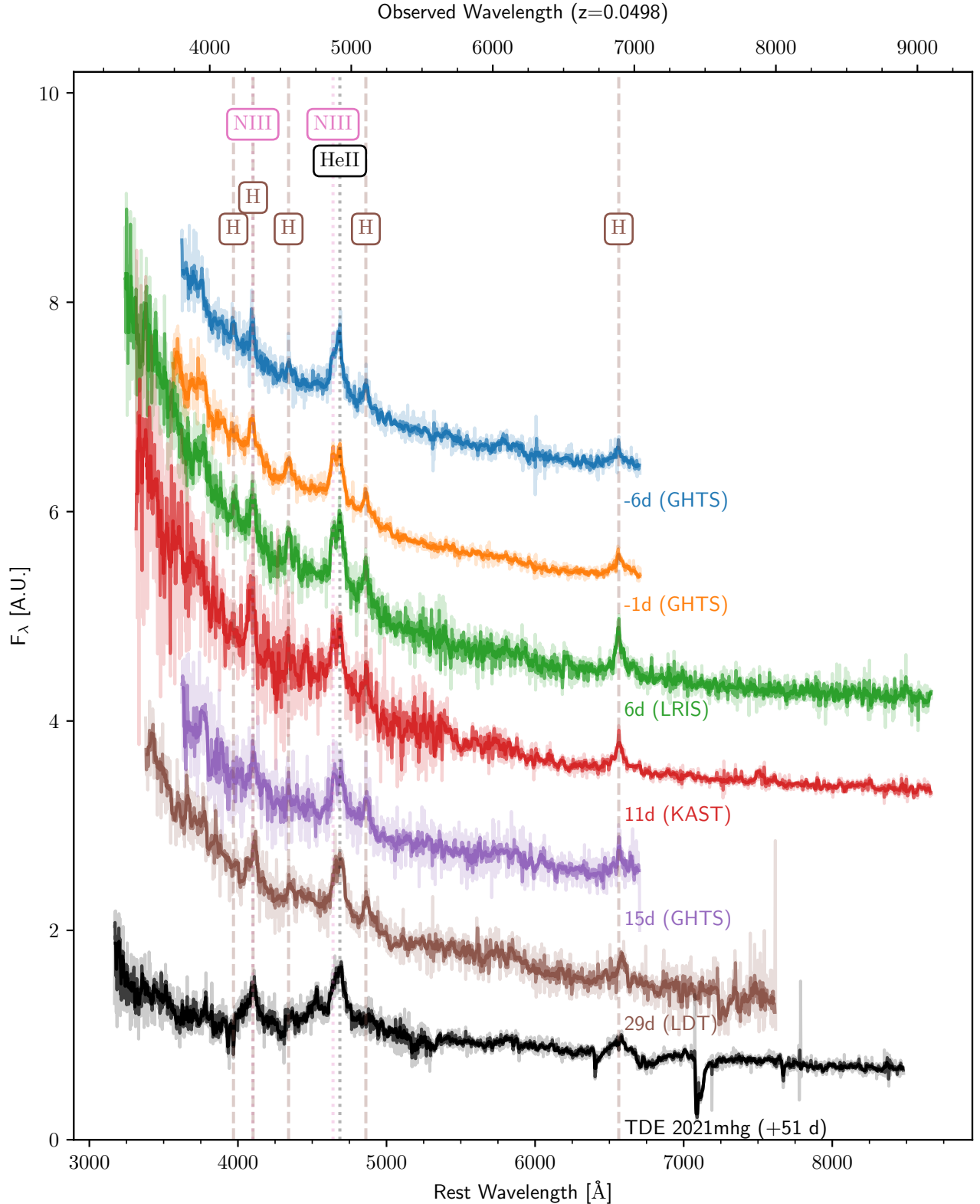


Figure 3. Spectral sequence of TDE 2025abcr, with times given in rest frame days relative to the peak date. The source exhibits a blue continuum with little apparent cooling, broad H lines and a blended feature of He II ($\lambda 4686$) and N III ($\lambda 4640$). A comparison spectrum of TDE 2021mhg (M. Chu et al. 2021), a TDE belonging to the same TDE-H+He spectral subclass at a similar phase, is shown in black at the bottom of the figure. The spectral features of TDE 2025abcr resemble this and other known TDEs.

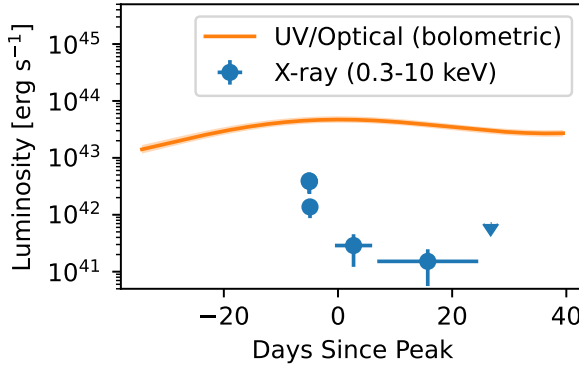


Figure 4. Bolometric luminosity (orange) from the UV/optical blackbody fit, alongside the X-ray detections (blue circles) and upper limits (blue triangles).

uncertainties of the inferred parameters. We find no evidence for intrinsic neutral hydrogen absorption ($\mathrm{NH}_{\mathrm{int}} < 0.5 \times 10^{22} \mathrm{cm}^{-2}$) and therefore fix the absorption to the Galactic value in the direction of TDE 2025abcr ($\mathrm{NH} = 1.55 \times 10^{20} \mathrm{cm}^{-2}$; [HI4PI Collaboration et al. 2016](#)). The metal abundances are set to Solar values with `wilm`. We find that the best-fitting model under-estimates the emission at energies > 0.7 keV. We thus update our model to include the contribution of a “Comptonization tail” (i.e., `tbabs*zashift*simpl*ezdiskbb`).²⁵ Within `simpl` ([J. F. Steiner et al. 2009](#)) a hard power-law component with a spectral photon index Γ is formed as a result of inverse Compton up-scattering of a fraction f_{sc} of the initial thermal seed photon population. Due to the limited statistics, we adopt $\Gamma = 2.5$ as found in other TDEs (e.g., [Y. Yao et al. 2025](#)), and fit the other parameters. We infer a disk maximum temperature $k_b T_{max} = 41_{-14}^{+5.0}$ eV and $f_{sc} = 1.7_{-1.5}^{+0.3} \times 10^{-3}$. The 0.3–10 keV absorbed (unabsorbed) flux is $3.5_{-0.5}^{+0.7} \times 10^{-13} \mathrm{erg s}^{-1} \mathrm{cm}^{-2}$ ($4.6_{-0.7}^{+0.9} \times 10^{-13} \mathrm{erg s}^{-1} \mathrm{cm}^{-2}$), corresponding to an unabsorbed luminosity of $L_X = 2.75_{-0.42}^{+0.54} \times 10^{42} \mathrm{erg s}^{-1}$.

We conclude that TDE 2025abcr initially shows the very soft X-ray emission that is a hallmark feature of TDEs, but this fades rapidly. Fast-fading X-ray emission was also observed for TDE 2019dsg ([R. Stein et al. 2021](#)) and TDE 2022dsb ([A. Malyali et al. 2024](#)), and has been previously attributed to obscuration of the X-ray-emitting region by optically-thick stellar debris. However, the very rapid fading of the soft X-ray component of TDE 2025abcr (a factor of ~ 3 over the course of ~ 4 hours) is exceptional. The X-ray variability of TDE

²⁵ We note that adding the contribution of the Comptonization tail has minimal effects on the best-fitting temperature value and flux.

2025abcr warrants further investigation that is beyond the scope of this paper.

3.7. Radio Observations

We observed the field of TDE 2025abcr with the Karl G. Jansky Very Large Array (VLA) on November 12, 2025, roughly 2 days before optical peak, under our dedicated program for off-nuclear TDEs (25B-109; PI: Sfaradi). This observation was conducted in X-band, with a central frequency of 10 GHz. We used 3C48 as an absolute flux and bandpass calibrator and J0204-1701 as a phase calibrator. We used the Common Astronomy Software Applications (CASA; [T. C. Team et al. 2022](#)) packages and the VLA calibration pipeline to flag and calibrate the data, and applied additional flagging manually. We used the CASA task `TCLEAN` to produce clean images of the field, and the CASA task `IMSTAT` to calculate the image rms.

No radio emission is detected in the 10 GHz band at the position of the TDE and at the center of the host galaxy down to a 3σ upper limit of $14 \mu\mathrm{Jy}$. This translates to a 3σ specific luminosity upper limit of $L_\nu \leq 8.3 \times 10^{26} \mathrm{erg s}^{-1} \mathrm{Hz}^{-1}$ at the distance of TDE 2025abcr. For comparison, the first radio bright off-nuclear TDE 2024tvd was initially not detected in the 10 GHz band down to a similar 3σ depth of $L_\nu \leq 8 \times 10^{26} \mathrm{erg s}^{-1} \mathrm{Hz}^{-1}$, about 90 days after optical discovery ([I. Sfaradi et al. 2025](#)). Late observations of TDE 2024tvd revealed a late-time brightening and a peak luminosity of $L_\nu \sim 10^{29} \mathrm{erg s}^{-1} \mathrm{Hz}^{-1}$. We therefore plan to continue monitoring TDE 2025abcr with the VLA.

4. DATA ANALYSIS

4.1. Modelling of TDE 2025abcr

4.1.1. UV/Optical Modelling

We follow the lightcurve analysis procedure introduced in [R. Stein et al. \(2024\)](#), performing an iterative Gaussian process fit to the lightcurve data. We correct for extinction using results from [E. F. Schlafly & D. P. Finkbeiner \(2011\)](#) and the extinction law from [E. L. Fitzpatrick \(1999\)](#). We model the multi-band lightcurve under the assumption that emission is thermal, and that it can be described by a blackbody spectrum with a temperature that evolves linearly in time (see e.g. [S. van Velzen et al. 2021](#)):

$$T(t, k, T_{peak}) = k \times (t - t_{peak}) + T_{peak} \quad (1)$$

where t_{peak} is the time of peak, T_{peak} is the temperature at peak and k is the cooling rate. Using this temperature T , the flux can be derived for any observed frequency, ν , and point in time, t :

$$f(\nu, T_{peak}, k, t) = \frac{B(\nu, T)}{B(\nu_0, T)} \times GP_{\nu_0}(t) \quad (2)$$

where $B(\nu, T)$ is the blackbody spectral radiance, GP_{ν_0} is the initial single-filter Gaussian Process fit and ν_0 is the central frequency of the g -band filter. The best-fit values for T_{peak} and k in Equation 2 are found using `scipy` minimisation (P. Virtanen et al. 2020).

As seen in Figure 2, the data are well described by a blackbody with a peak temperature of $T_{peak} = 30220 \pm 2120$ K and a varying inferred radius of order 10^{14} cm. We infer a peak bolometric luminosity of $4.71_{-0.59}^{+0.66} \times 10^{43}$ erg s $^{-1}$ on 2025-11-14, which we adopt as the peak date.

We can also estimate the mass of the BH which disrupted the star using the relation of A. Mummetry et al. (2024):

$$\log\left(\frac{M_{BH}}{M_{\odot}}\right) = 6.52 + 0.98 \log\left(\frac{L_{g,peak}}{10^{43} \text{erg s}^{-1}}\right) \quad (3)$$

with an intrinsic scatter of ~ 0.53 dex. Given the observed peak g -band luminosity of $\nu F_{\nu} = (3.66 \pm 0.34) \times 10^{42}$ erg s $^{-1}$, we estimate a BH mass of $10^{6.09 \pm 0.53} M_{\odot}$.

4.1.2. Comparison with known TDEs

We can use the procedure outlined in Section 4.1.1 to compare the properties of TDE 2025abcr with other known TDEs. For consistency, we repeat the analysis of TDE 2025abcr using only ZTF data, and then perform the same analysis for the sample of 30 TDEs discovered in ZTF-I (E. Hammerstein et al. 2023). The best-fit values for TDE 2025abcr therefore deviate slightly from those in Section 4.1.1, due to the absence of UV data. After performing the lightcurve fitting, we extract the key classifier features used by `tdescore` such as rise time and fade time. The results of these fits are shown in Figure 5.

The general lightcurve properties of TDE 2025abcr are consistent with the overall sample of nuclear TDEs in most key properties: inferred peak temperature and cooling rate, rise time and fade time. There is one clear difference: TDE 2025abcr has a lower peak g -band absolute magnitude ($M_g = -17.6$) than typical optical TDEs. There are other optical TDEs with comparable luminosities, but the source is clearly far below the population median. However, the peak magnitude remains significantly brighter than the transient optical counterpart ($M_g = -14.6$) to the X-ray-selected IMBH-TDE EP240222A/AT 2024agqv (C. C. Jin et al. 2025). TDE 2025abcr thus qualitatively resembles a faint TDE from the broader optically-selected massive BH/TDE population, much more than it resembles EP240222A.

4.2. Modelling of the host galaxy

4.2.1. Stellar Population Synthesis

We analyzed the host galaxy of TDE 2025abcr, WISEA J014656.04-152214.7. We used `galsynths`²⁶ (R. D. Stein 2025), an open-source Dockerized python package for automated galaxy SED fitting built using `prospector` (B. D. Johnson et al. 2021) and `astroquery`. Photometry of the host galaxy was downloaded from GALEX (D. C. Martin et al. 2005), SDSS (D. G. York et al. 2000), 2MASS (M. F. Skrutskie et al. 2006) and WISE (E. L. Wright et al. 2010). The model provides a good fit to the galaxy SED. The resultant best-fit parameters are summarized in Appendix Table 5, while the full corner plot is shown in Appendix Figure 11. The most important conclusion from the fit is the tight constraint on the inferred surviving stellar mass of the galaxy: $M_{\star} = 10^{11.18 \pm 0.03} M_{\odot}$. From galaxy scaling relations of J. E. Greene et al. (2020) for early-type galaxies, we would expect a central BH mass of $10^{8.82 \pm 0.65} M_{\odot}$. The host galaxy is therefore very massive, much more so than typical TDE hosts (see e.g. E. Hammerstein et al. 2023) but consistent with other off-nuclear TDEs (see Appendix Table 2).

4.2.2. Galaxy Profile Modelling

In order to search for evidence of previous merger activity or the presence of an additional nuclear star cluster (NSC) offset from the host galaxy center, we undertook modeling of the coadded g , r and z band imaging available from the Legacy Survey Data Release 10 (A. Dey et al. 2019) using the `Scarlet` multi-band scene modeling software²⁷ (P. Melchior et al. 2018). Note that the typical size of NSCs is 5 pc (N. Neumayer et al. 2020), which corresponds to 6 mas at $z = 0.05$. If an off-nuclear NSC exists and is above the sensitivity limit, we only expect it to be detected as a point source.

The LS DR10 has a 0.262'' pixel scale and depths of $g \approx 24.7$, $r \approx 23.9$, $z \approx 23.0$ mag. For the LS DR10 models, we provided `Scarlet` with the point spread function (PSF) model images provided by the data release. We ran `Source Extractor` (E. Bertin & S. Arnouts 1996) to identify all sources detected over a 5σ threshold. We required that all background galaxy models be monotonically decreasing — but not radially symmetric — and that they have the same morphology in each band (such that the SED does not vary in different regions of the galaxy). This enables us to avoid any assumptions about the galaxies following an ana-

²⁶ <https://github.com/robertdstein/galsynths>

²⁷ <https://pmelchior.github.io/scarlet/>

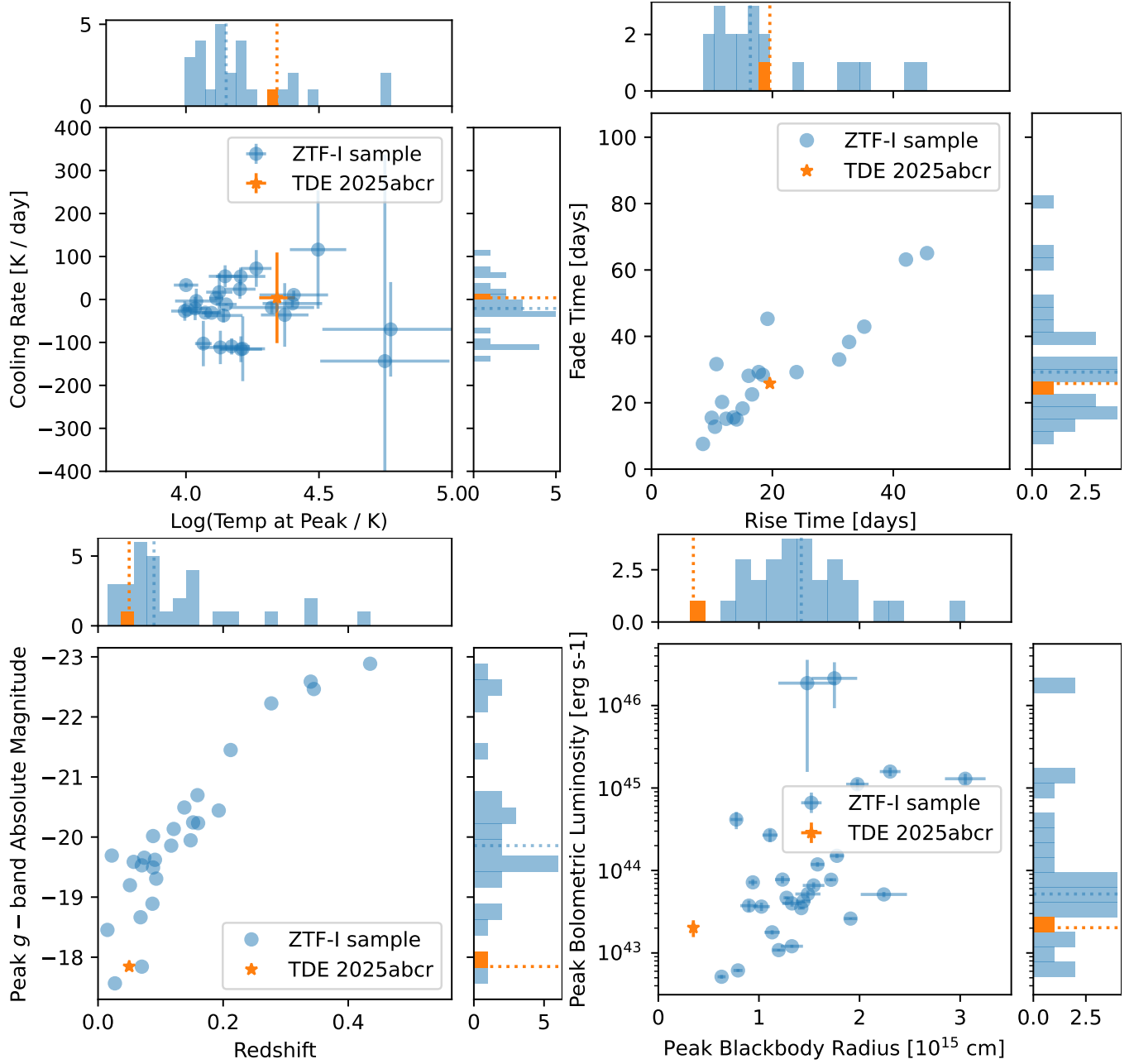


Figure 5. Comparison of the optical lightcurve properties of TDE 2025abcr (in orange) and the sample of TDEs reported in E. Hammerstein et al. (2023) (in blue). The median of each distribution is illustrated with a dashed line. The best-fit values for TDE 2025abcr differ slightly from those in Figure 2, because no UV data was included in these fits. **Top Left:** Best-fit peak temperature versus cooling rate for TDEs, using the thermal model outlined in Section 4.1.1 and fitting only ZTF photometric data. **Top Right:** Best-fit rise time and fade time for the same sample and fitting procedure, with the time defined as days between peak magnitude and 0.5 magnitude below peak. **Lower Left:** Redshift versus peak absolute g -band magnitude. **Lower Right:** Bolometric luminosity versus blackbody radius. TDE 2025abcr has a typical peak temperature and cooling rate, as well as a typical rise and fade time. In these lightcurve properties, the source is therefore an unremarkable optical TDE. However, the source has a low peak absolute g -band magnitude compared to other ZTF TDEs. As a relatively hot blackbody, TDE 2025abcr has a much lower inferred blackbody radius than the overall ZTF population. This supports the interpretation that TDE 2025abcr is a normal optical TDE but arises from a $\sim 10^6 M_\odot$ BH, as argued in more detail in Section 4.1.1.

lytical galaxy profile. For the primary host galaxy, we applied a double pseudo-Sérsic profile (D. N. Spergel 2010) as the stronger constraints on profile shape enabled improved modeling of the diffuse emission in the galaxy disk in comparison to the non-parametric model. **Scarlet** was run to convergence to fit the multi-band SEDs and galaxy morphologies for the sources in the scene.

The best fit model, corresponding observations, and residuals are shown in Figure 6. The LS residuals show evidence of a disturbed morphology in the galaxy bulge, but do not show any excess point-like emission at the location of the TDE. In the LS g -band image, we estimate the limiting magnitude by determining the pixel variance of the residuals in a 30×30 pixel cutout centered on the TDE position. We determine a 3σ limiting magnitude of $g \approx 23.84$ mag, which implies that no NSC exists at the TDE position with an absolute g -band magnitude brighter than -12.78 mag.

Assuming a similar g -band mass-to-light ratio as EP240222A (C. C. Jin et al. 2025), which had a $10^7 M_\odot$ dwarf host at an absolute magnitude of -11.8 mag, we find a limit of $<10^{7.4} M_\odot$ for any dwarf galaxy at the position of TDE 2025abcr.

4.2.3. BH Mass from velocity dispersion

The Gaussian fit centroids of TDE 2025abcr’s broad H and He features closely agree with the redshift of the host WISEA J014656.04-152214.7, as derived from narrow galaxy lines. Using the broad $H\beta$ line, which is isolated and clearly resolved in all SOAR and LRIS spectra, we measure velocity differences between TDE 2025abcr and WISEA J014656.04-152214.7 to be negligible along our line of sight (mean 2 km s^{-1} , standard deviation 37 km s^{-1}).

Using the spectrum of WISEA J014656.04-152214.7, we fit the stellar continuum with the pPXF package (M. Cappellari 2023) using the line masking recommendations outlined in A. J. Barth et al. (2002) and the E-MILES stellar population synthesis templates (A. Vazdekis et al. 2016). Prior to fitting we convolved the template spectra to match the instrumental resolution of GHTS (with a median $R \sim 1430$ corresponding to a median $\sigma_{\text{instrumental}} \approx 210 \text{ km s}^{-1}$). We measure a velocity dispersion of $\sigma = 324 \pm 14 \text{ km s}^{-1}$. Using the $M_\bullet - \sigma$ relation (L. Ferrarese & D. Merritt 2000; K. Gebhardt et al. 2000) with updated coefficients from J. Kormendy & L. C. Ho (2013) we estimate the central BH mass of WISEA J014656.04-152214.7 to be $\log(M_{\text{BH}}/M_\odot) = 9.41 \pm 0.31$, where the uncertainty includes the 0.29 dex intrinsic scatter from the $M_{\text{BH}} - \sigma$

relation. This is consistent with the independent estimate of $10^{8.82 \pm 0.65} M_\odot$ described in Section 4.2.1.

4.2.4. Is the host an active galaxy?

We consider whether the host of TDE 2025abcr is an active galaxy, because this would conclusively prove that at least one massive BH remains present in the galaxy nucleus. We see no evidence of this, after testing the following common AGN indicators:

- There are no AGN-associated signatures in the host galaxy spectrum (e.g. [O III], broad Balmer lines).
- There is no detection of the galaxy in either our radio or X-ray observations, as would be expected for most AGN.
- There are no indications of previous nuclear variability in ZTF data.
- The WISE mid-infrared colors of the galaxy are not AGN-like ($W1 - W2 = -0.03$) (D. Stern et al. 2012)

While we cannot exclude the possibility of low-level AGN activity, we do not see any evidence supporting this. Instead, our observations suggest that WISEA J014656.04-152214.7 is a quiescent early-type galaxy. Therefore, in contrast to the off-nuclear TDE 2024tv where radio emission from the central BH was detected (Y. Yao et al. 2025), we cannot prove that a BH is still present at the center of the host galaxy of TDE 2025abcr.

4.3. The rate of offset TDEs

TDE 2025abcr peaked in ZTF data with an apparent g -band magnitude of 18.9 mag, which was too faint to be selected by systematic transient classification programs such as the ZTF Bright Transient Survey (BTS; C. Fremling et al. 2020; D. A. Perley et al. 2020). However, given that the observed properties of TDE 2025abcr (clear off-nuclear location, moderate luminosity, slow evolution) are similar to core-collapse SNe, it is very likely that brighter off-nuclear TDEs would have been classified by BTS. As no comparable transient was discovered before, we can conclude that TDE 2025abcr-like transients must be rare.

As of December 2025, the ZTF BTS survey²⁸ has identified 24 TDEs passing SN-like cuts amongst a larger sample of 4728 SN-like transients brighter than 18.5

²⁸ <https://sites.astro.caltech.edu/ztf/bts/bts.php>

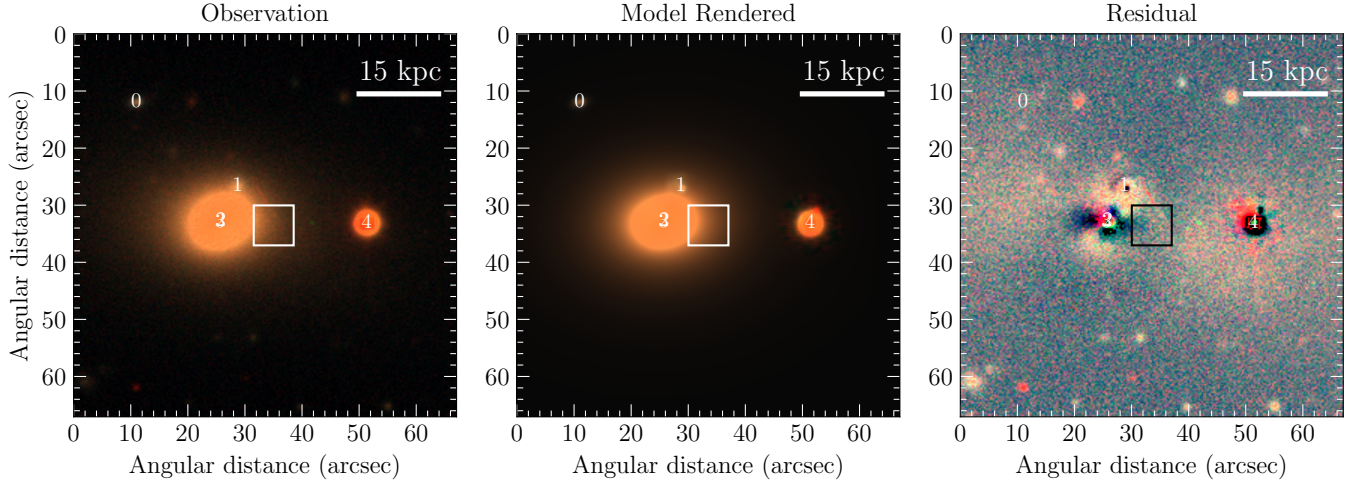


Figure 6. Scarlet scene model from Legacy Survey DR10 imaging (*grz*). Each labeled source was modeled as a monotonically decreasing profile except for the host galaxy, which was modeled by a double pseudo-Sérsic in order to best account for the diffuse extended emission. We show the model rendered to match the LS imaging (left), the coadded LS *grz* image (center), and the data–model residual (right). The central box showed the region used to estimate an upper limit on a NSC cluster associated with the TDE position.

mag, a regime in which spectroscopic completeness is $\sim 93\%$. None of these 4728 transients resemble TDE 2025abcr. We can conservatively place an upper limit at 90% confidence on the expected number of highly offset TDEs in the BTS sample at $N < 2.3$ assuming Poisson counting uncertainties (N. Gehrels 1986). We can therefore conservatively constrain the rate of high-offset TDEs such as TDE 2025abcr to less than $f \lesssim 2.3/24 = 9.6\%$ of the ‘nuclear’ TDE rate, where nuclear in this context means TDEs without a resolved offset in ZTF data.

It is difficult to measure the overall rate of off-nuclear optical TDEs, because we expect that some will not have resolvable offsets in ZTF data. However, we can say that at least one of the 24 BTS TDEs was confirmed to be offset (TDE 2024tvd). We can therefore place a lower limit on the overall rate of offset TDEs. A single detection implies a lower limit at 90% confidence of $N > 0.05$. We can therefore say that at least $f \gtrsim 0.05/24 = 0.2\%$ of all TDEs are offset, though the true fraction may be substantially higher. Our limit is consistent with the fraction of off-nuclear X-ray-selected TDEs (I. Grotova et al. 2025).

5. THE ORIGIN OF TDE 2025abcr

By definition, TDEs occur at the position of BHs. We can therefore be sure that a massive BH is present in the outskirts of the massive galaxy, possibly originating from a galaxy merger. Following a merger, dynamical friction should eventually lead to a compact supermas-

sive BH binary (M. C. Begelman et al. 1980), but this process can take billions of years. In the interim, tidal stripping will progressively consume the lighter galaxy, leaving an ‘orphan’ BH with ever-fewer stars that remains bound to the larger galaxy and slowly spirals inwards.

Ultimately the BHs will form a compact binary that can remain stable for long periods. Any incoming massive BHs from new mergers that approach a pre-existing binary will undergo complex three-body interactions that lead to the ejection of the least massive BH. These binaries will draw closer and may merge via gravitational wave emission, detectable via pulsar timing arrays (see S. R. Taylor 2025, for a recent review) and LISA (P. Amaro-Seoane et al. 2017). Even after an eventual binary merger, nuclear recoil following a merger could lead to the ejection of the new central BH (see e.g. M. Campanelli et al. 2007; L. Blecha et al. 2016).

Merging galaxies may host a pre-existing nuclear star cluster, while ejected BHs may also partially retain a nuclear star cluster (see e.g. S. Komossa & D. Merritt 2008; N. Stone & A. Loeb 2012; F. K. Liu & X. Chen 2013; N. Khonji et al. 2025). The intrinsic TDE rate will depend strongly on the presence of a star cluster accompanying the BH, and they may be considerably less frequent than for nuclear BHs (see e.g. S. Komossa & D. Merritt 2008; N. Stone & A. Loeb 2012; F. K. Liu & X. Chen 2013; S. Li et al. 2019). Beyond these merger-related channels, globular clusters (GCs) formed in-situ may host IMBHs of order $10^{3-4} M_{\odot}$ (N. Lützgendorf et al. 2013) along-

side numerous stars. It is therefore natural to expect that TDEs could occur in GCs (E. Ramirez-Ruiz & S. Rosswog 2009; J.-H. Chen & R.-F. Shen 2018; G. Fragione et al. 2018; V. L. Tang et al. 2024), and this would be an additional channel for off-nuclear TDEs.

To summarise, we consider the following formation channels for an offset BH:

- A - an in-spiralling BH from a major merger
- B - an in-spiralling BH from a minor merger
- C - a BH from a previous merger that was dynamically ejected by three-body interactions in the galaxy nucleus
- D - a ‘recoiling’ central BH ejected from a now-empty galaxy nucleus
- E - an IMBH hosted by a GC

The key results from our modelling are that TDE 2025abcr appears to be a TDE with a parent BH mass of $10^{6.09 \pm 0.53} M_{\odot}$, with no evidence of an underlying dwarf galaxy or star cluster. The host galaxy is massive, with an inferred BH mass much higher than the TDE BH mass. Given this context, it is clear that both scenario A and D are not viable owing to significant mismatch between TDE-BH and host-BH mass. Moreover, the inferred central BH mass ($10^{8.82 \pm 0.65} M_{\odot}$) from the host galaxy is so large that it is very unlikely to produce a TDE even with extreme spin values.

For scenario E, GCs span a range of absolute magnitudes peaking at $M_V = -7.5$ and not typically exceeding $M_V = -11$ (M. Rejkuba 2012). We would therefore not expect to detect a GC in archival LS imaging, and our non-detection would therefore be consistent with the GC scenario. However, the inferred TDE-BH mass ($10^{6.09 \pm 0.53} M_{\odot}$) is substantially larger than would be expected for a globular cluster. $M-\sigma$ scaling relations have been found to hold for GCs (N. Lützgendorf et al. 2013), and with our absolute magnitude limit of -12.78 we would expect a BH mass no more massive than $10^{4.8} M_{\odot}$. Using the upper end of observed globular clusters ($M_V \approx -11$), we would expect $\lesssim 10^{4.3} M_{\odot}$. In both cases, there is considerable tension with the large inferred TDE-BH mass of TDE 2025abcr, and we therefore consider scenario E to not be a viable explanation.

For a recent minor merger, we can apply a similar argument, and conclude that our non-detection of a host would exclude a dwarf galaxy hosting a $10^6 M_{\odot}$ BH. However, tidal stripping of stars following a merger will lead to a dimming of the galaxy over time, such that the central BH will be substantially heavier than expected based on stellar luminosity.

A historical minor merger (Scenario B) would therefore remain a plausible origin, alongside Scenario C. It is interesting to note that the host galaxy of the transient is massive, as this is consistent with predictions that the number of wandering BHs will scale linearly with galaxy halo mass (A. Ricarte et al. 2021b). These arguments are summarised in Table 1.

We can also consider potential offsets in redshift between the transient itself and the host itself, due to the motion of the transient. For the dynamical ejection scenario, a single BH can be ejected with velocities of $\sim 1000 \text{ km s}^{-1}$ (L. Hoffman & A. Loeb 2007). A BH ejected from the nucleus would likely experience significant deceleration from dynamical friction before reaching a 10.3 kpc offset and/or could be travelling on a trajectory perpendicular to our line of sight. As such, the observed low velocity offset only provides as a weak constraint rather than evidence against a merger kick or dynamical three-body interaction.

6. DISCUSSION AND CONCLUSION

To summarise, TDE 2025abcr is an ML-selected off-nuclear TDE with properties broadly consistent with typical nuclear optical TDEs. Our UV, X-ray and spectroscopic observations confirm unambiguously that the source is indeed a TDE rather than an AGN flare or SN. The parent BH must be massive ($10^{6.09 \pm 0.53} M_{\odot}$), but there is no evidence of emission at this location in archival imaging. The BH may have therefore originated in a previous minor merger or a dynamical ejection following a nuclear three-body interaction.

Further late-time observations will shed more light on the properties of TDE 2025abcr and its origin. In particular, the TDE-BH mass can be measured more precisely with observations of the late UV-optical plateau (A. Mummery et al. 2024) which appears ubiquitous in optical TDEs (S. van Velzen et al. 2019), and potentially through joint modelling of any late-time X-ray emission that might be detected (M. Guolo et al. 2025). Moreover, the presence of any underlying host could be tested through deep late-time imaging at the position of TDE 2025abcr, after the transient itself has faded. This would constrain the viability of the ‘minor merger’ origin channel for the BH. If no underlying source is found, we would instead favour a dynamical ejection origin for TDE 2025abcr.

With the discovery of TDE 2025abcr, we can already consider patterns in the enlarged sample of off-nuclear TDEs discovered to date. A list of well-studied examples is presented in Appendix Table 2. All occur in very massive galaxies, which is consistent with theoretical predictions that the number of wandering BHs in a galaxy

	Scenario	Arguments In Favor	Arguments Against	Viable?
A	Major Merger	/	TDE-BH mass << Host-BH Mass	N
B	Minor Merger	Explains TDE-BH Mass Consistent with other off-nuclear TDEs	No bright underlying host	Y
C	Dynamical Ejecta MBH	Explains TDE-BH mass Consistent with TDE 2024tvd	No redshift offset	Y
D	Recoiling MBH	No direct evidence of BH in nucleus	TDE-BH mass << Host-BH mass	N
E	Globular Cluster	Host should be too faint to detect	TDE-BH mass is too large	N

Table 1. Scenarios for the origin of the BH which generated TDE 2025abcr. Given the large difference between the inferred TDE-BH mass ($10^{6.09 \pm 0.53} M_{\odot}$) and the inferred galaxy BH mass ($10^{8.82 \pm 0.65} M_{\odot}$), we can exclude a major merger and a recoiling MBH origin. The inferred TDE-BH mass is too large for a GC origin. However, a minor merger and a dynamical ejection remain viable.

scale with the host halo mass (A. Ricarte et al. 2021b). However, the other properties of the flares are grouped into distinct categories:

- **Candidate IMBH-TDEs in dwarf galaxies:** so far these are mostly X-ray-selected TDEs which occur at the center of dwarf satellites. They exhibit very faint optical emission, consistent with expectations from scaling relations (A. Mummery et al. 2024) and simulations (P. Martire et al. 2025) that IMBH-TDEs should be intrinsically low-luminosity in the optical. This category includes EP240222a, 3XMM J2150, and HLX-1. It excludes TDE 2025abcr owing to its bright optical emission and relatively high inferred TDE-BH mass.
- **Low-Offset ($\lesssim 3$ kpc) Optical TDEs:** TDE 2024tvd is the prototypical example of this group, and appears to be an unexceptional optical TDE with typical thermal emission. It is likely that, given the poor spatial resolving power of ground-based optical telescopes, a substantial fraction of these TDEs will not be identified as off-nuclear. Some of the known optical TDEs may in fact belong to this category.
- **High-Offset ($\gtrsim 3$ kpc) Optical TDEs:** TDE 2025abcr is the first example of this group. Much like low-offset optical TDEs, the multi-wavelength properties appear similar to optically-selected nuclear TDEs. We can state with confidence that high-offset optical TDEs must be intrinsically rare ($< 10\%$ of the nuclear TDE rate).

Additional low-offset optical TDEs could be identified with systematic multi-wavelength follow-up, though this will remain impractical to conduct for all newly identified TDEs. One simple alternative would be to target any TDEs occurring in a very massive galaxy with

$M_{BH} \gtrsim 10^8 M_{\odot}$, as has been proposed for searches targeting massive BH binaries (see e.g. B. Mockler et al. 2023). More broadly, searches could focus on TDEs which have an inferred BH mass that deviates substantially from predictions of the TDE scaling relation of A. Mummery et al. (2024). Both techniques would have reliably identified both TDE 2024tvd and TDE 2025abcr as clear outliers.

Finding additional high-offset TDEs like TDE 2025abcr is much more straightforward. Photometric selection with `tdescore` is already effective in reducing the SN contamination, and the offset nature can be easily identified by the imaging in all-sky surveys. The very large projected offset of TDE 2025abcr is encouraging for the off-nuclear TDE discovery prospects with the *Vera C. Rubin Observatory* (Ž. Ivezić et al. 2019). $\mathcal{O}(10)$ kpc offsets should be easily resolvable ($> 1''$) even at a redshift of $z = 1$. Given that Rubin is expected to identify thousands of nuclear TDEs each year (K. Bricman & A. Gomboc 2020; M. Karmen et al. 2026), we can expect many more off-nuclear TDEs will be discovered in the near future.

ACKNOWLEDGMENTS

Based on observations obtained with the Samuel Oschin Telescope 48-inch and the 60-inch Telescope at the Palomar Observatory as part of the Zwicky Transient Facility project. ZTF is supported by the National Science Foundation under Award #2407588 and a partnership including Caltech, USA; Caltech/IPAC, USA; University of Maryland, USA; University of California, Berkeley, USA; Cornell University, USA; Drexel University, USA; University of North Carolina at Chapel Hill, USA; Institute of Science and Technology, Austria; National Central University, Taiwan, and the German Center for Astrophysics (DZA), Germany. Operations are conducted by Caltech's Optical Observatory

(COO), Caltech/IPAC, and the University of Washington at Seattle, USA.

SED Machine is based upon work supported by the National Science Foundation under Grant No. 1106171.

The Gordon and Betty Moore Foundation, through both the Data-Driven Investigator Program and a dedicated grant, provided critical funding for SkyPortal.

Some of the data presented herein were obtained at Keck Observatory, which is a private 501(c)3 non-profit organization operated as a scientific partnership among the California Institute of Technology, the University of California, and the National Aeronautics and Space Administration. The Observatory was made possible by the generous financial support of the W. M. Keck Foundation. The authors wish to recognize and acknowledge the very significant cultural role and reverence that the summit of Maunakea has always had within the Native Hawaiian community. We are most fortunate to have the opportunity to conduct observations from this mountain.

A major upgrade of the Kast spectrograph on the Shane 3 m telescope at Lick Observatory, led by Brad Holden, was made possible through gifts from the Heising-Simons Foundation, William and Marina Kast, and the University of California Observatories. Research at Lick Observatory is partially supported by a generous gift from Google.

This work made use of data supplied by the UK Swift Science Data Centre at the University of Leicester.

This paper contains data obtained at the Wendelstein Observatory of the Ludwig-Maximilians University Munich. We thank Christoph Ries for carrying out the observations. Funded in part by the Deutsche Forschungsgemeinschaft (DFG, German Research Foundation) under Germany's Excellence Strategy – EXC-2094/2 – 390783311.

The national facility capability for SkyMapper has been funded through ARC LIEF grant LE130100104 from the Australian Research Council, awarded to the University of Sydney, the Australian National University, Swinburne University of Technology, the University of Queensland, the University of Western Australia, the University of Melbourne, Curtin University of Technology, Monash University and the Australian Astronomical Observatory. SkyMapper is owned and operated by The Australian National University's Research School of Astronomy and Astrophysics. The survey data were processed and provided by the SkyMapper Team at ANU. The SkyMapper node of the All-Sky Virtual Observatory (ASVO) is hosted at the National Computational Infrastructure (NCI). Development and support of the SkyMapper node of the ASVO has been funded

in part by Astronomy Australia Limited (AAL) and the Australian Government through the Commonwealth's Education Investment Fund (EIF) and National Collaborative Research Infrastructure Strategy (NCRIS), particularly the National eResearch Collaboration Tools and Resources (NeCTAR) and the Australian National Data Service Projects (ANDS).

The National Radio Astronomy Observatory (NRAO) is a facility of the National Science Foundation operated under cooperative agreement by Associated Universities, Inc. We thank the NRAO for carrying out the Karl G. Jansky Very Large Array (VLA) observation.

AUTHOR CONTRIBUTIONS

RS developed the `tdescore` scanning infrastructure, coordinated multi-wavelength follow-up and led writing of this manuscript. JC obtained the classification spectrum of TDE 2025abcr and led spectroscopic analysis. CW contributed the galaxy profile modelling. RM led the Swift-XRT data analysis. XJH, MB, DG, BO and AP provided Wendelstein imaging and analysis. IS contributed radio observations and analysis. RS, JC, RM, XJH, IS, IA, RC, SG, YY, MJG, EH and JJS discovered TDE 2025abcr as members of the ZTFBH working group. RS, SG, SBC, JR and SV contributed LDT imaging and spectroscopy. JC and IA contributed GHTS spectroscopy. RC and EH contributed Kast and LRIS spectroscopy. GM and IC contributed high-cadence imaging and analysis. EB, MJG, SLG, MMK, JP, RR, BR and JS contributed to the development and operation of ZTF. All authors contributed to the development of this work.

Facilities: PO:1.2m (ZTF), Hale (protoCerberus), Keck:I (LRIS), LDT (DeVeny, LMI), PO:1.5m (SEDM), SOAR (Goodman), Swift (XRT, UVOT), VLA, WO:2m (3KK)

Software: `astroquery` (B. D. Johnson et al. 2021), `emcee` (D. Foreman-Mackey et al. 2013), `HEASoft`, `galsynthspect` (R. D. Stein 2025), `mirar` (R. D. Stein et al. 2025), `prospector` (B. D. Johnson et al. 2021), `SCAMP` (E. Bertin 2006), `scarlet` (P. Melchior et al. 2018), `Source Extractor` (E. Bertin & S. Arnouts 1996), `swiftools`, `tdescore` (R. Stein et al. 2024), `uvotredux` (R. D. Stein & J. Carney 2025)

APPENDIX

Date	Phase [days]	Instrument	Filter [AB]	Mag [AB]	Mag Err [AB]	Limiting Mag
2025-10-11T08:01:30.000	-32.7d	ZTF	r	20.71	0.32	19.93
2025-10-11T09:03:15.998	-32.7d	ZTF	g	19.99	0.28	19.48
2025-10-13T06:42:19.996	-30.9d	ZTF	g	20.51	0.27	20.22
2025-10-13T09:04:32.998	-30.8d	ZTF	r	20.81	0.29	20.11
2025-10-17T07:51:44.001	-27.0d	ZTF	r	20.41	0.23	20.00
2025-10-17T09:20:47.996	-26.9d	ZTF	g	19.79	0.24	19.79
2025-10-18T10:04:42.004	-26.0d	ZTF	r	19.96	0.20	19.69
2025-10-19T07:29:10.000	-25.1d	ZTF	r	20.31	0.25	20.21
2025-10-19T07:57:41.999	-25.1d	ZTF	g	19.83	0.17	20.29
2025-10-20T10:04:44.000	-24.1d	ZTF	r	20.38	0.27	19.97
2025-10-21T08:15:31.000	-23.2d	ZTF	g	19.76	0.16	20.27
2025-10-21T09:16:45.998	-23.1d	ZTF	r	20.04	0.19	20.08
2025-10-23T08:03:28.999	-21.3d	ZTF	r	20.11	0.27	19.99
2025-10-25T06:32:10.997	-19.4d	ZTF	r	19.83	0.14	20.28
2025-10-25T07:37:55.001	-19.4d	ZTF	g	19.51	0.13	20.41
2025-10-27T06:43:57.999	-17.5d	ZTF	g	19.39	0.12	20.33
2025-10-27T08:39:23.003	-17.5d	ZTF	r	19.56	0.14	19.99
2025-10-28T06:48:13.000	-16.6d	ZTF	r	19.61	0.15	20.00
2025-10-29T05:07:29.001	-15.7d	ZTF	r	19.80	0.17	19.96
2025-10-29T07:02:03.002	-15.6d	ZTF	g	19.21	0.13	20.26
2025-10-31T07:01:41.998	-13.7d	ZTF	r	19.87	0.17	20.01
2025-11-02T05:32:58.004	-11.9d	ZTF	g	19.24	0.19	19.37
2025-11-02T08:07:42.997	-11.8d	ZTF	r	19.61	0.21	19.48
2025-11-04T04:57:02.998	-10.0d	ZTF	g	19.17	0.20	19.06
2025-11-04T06:30:18.003	-9.9d	ZTF	r	19.17	0.16	19.27
2025-11-05T04:34:00.434	-9.0d	SEDM	r	/	/	19.15
2025-11-07T06:01:46.998	-7.1d	ZTF	g	19.03	0.17	19.21
2025-11-07T07:31:03.003	-7.0d	ZTF	r	19.23	0.22	19.26
2025-11-08T05:14:23.004	-6.2d	ZTF	g	19.14	0.14	19.51
2025-11-08T07:22:57.003	-6.1d	ZTF	r	19.52	0.15	19.72
2025-11-09T05:05:42.081	-5.2d	SEDM	r	19.49	0.11	20.23
2025-11-09T05:07:39.999	-5.2d	ZTF	g	18.99	0.11	19.73
2025-11-09T05:59:40.154	-5.2d	SEDM	i	/	/	17.99
2025-11-09T07:04:56.001	-5.1d	ZTF	r	19.31	0.17	19.57
2025-11-09T16:36:04.308	-4.8d	UVOT	UVW2	18.01	0.05	21.92
2025-11-09T18:25:27.604	-4.7d	UVOT	UVM2	18.36	0.06	22.22
2025-11-09T18:54:39.851	-4.7d	UVOT	UVW1	18.37	0.06	21.38
2025-11-09T18:56:44.076	-4.7d	UVOT	U	18.50	0.06	21.00
2025-11-10T03:38:13.998	-4.3d	ZTF	r	19.38	0.17	19.61
2025-11-10T05:47:26.998	-4.2d	ZTF	g	19.09	0.13	19.93
2025-11-11T08:46:55.998	-3.2d	ZTF	g	19.02	0.14	19.31
2025-11-11T20:56:34.368	-2.7d	Wendelstein 3KK	Ks	/	/	20.04
2025-11-11T21:35:15.072	-2.6d	Wendelstein 3KK	J	/	/	20.47
2025-11-15T02:12:11.703	0.4d	UVOT	UVW2	18.00	0.05	22.24

2025-11-17T18:18:58.672	2.9d	UVOT	UVW1	18.30	0.06	21.42
2025-11-17T18:20:07.196	2.9d	UVOT	U	18.46	0.09	20.51
2025-11-17T18:23:36.308	2.9d	UVOT	UVW2	17.98	0.05	22.20
2025-11-17T18:28:41.054	2.9d	UVOT	UVM2	18.33	0.06	22.10
2025-11-20T14:17:11.864	5.6d	UVOT	UVW1	18.45	0.07	21.21
2025-11-20T14:19:13.981	5.6d	UVOT	U	18.62	0.09	20.57
2025-11-20T14:23:01.595	5.6d	UVOT	UVW2	18.04	0.05	22.02
2025-11-20T14:29:42.328	5.6d	UVOT	UVM2	18.31	0.06	22.00
2025-11-24T04:14:34.376	9.0d	UVOT	UVW1	18.48	0.07	21.16
2025-11-24T04:16:15.518	9.0d	UVOT	U	18.57	0.09	20.57
2025-11-24T04:20:23.483	9.0d	UVOT	UVW2	18.11	0.05	21.96
2025-11-24T04:27:06.460	9.1d	UVOT	UVM2	18.37	0.05	22.10
2025-11-24T08:18:45.003	9.2d	ZTF	r	19.46	0.18	19.79
2025-11-26T05:33:06.998	11.0d	ZTF	g	19.24	0.14	20.01
2025-11-26T06:03:19.999	11.0d	ZTF	r	19.59	0.12	20.02
2025-11-26T17:37:43.214	11.5d	UVOT	UVM2	18.43	0.06	21.93
2025-11-26T18:50:26.884	11.5d	UVOT	UVW1	18.55	0.07	20.89
2025-11-26T18:53:10.043	11.5d	UVOT	U	18.51	0.09	20.54
2025-11-26T18:56:03.651	11.5d	UVOT	UVW2	18.14	0.05	21.76
2025-11-27T06:03:52.001	12.0d	ZTF	g	18.98	0.19	19.19
2025-11-28T22:53:45.341	13.6d	UVOT	UVW1	18.64	0.07	21.44
2025-11-28T22:54:57.649	13.6d	UVOT	U	18.55	0.09	20.61
2025-11-28T22:59:42.662	13.6d	UVOT	UVW2	18.22	0.05	22.20
2025-11-28T23:01:41.106	13.6d	UVOT	UVM2	18.53	0.07	21.66
2025-11-29T04:31:39.999	13.8d	ZTF	g	19.22	0.16	19.55
2025-11-29T06:34:14.998	13.9d	ZTF	r	19.46	0.17	19.54
2025-12-01T06:38:13.998	15.8d	ZTF	r	20.02	0.31	19.21
2025-12-02T02:05:42.184	16.6d	SEDM	i	/	/	19.38
2025-12-02T18:45:44.993	17.2d	UVOT	UVW1	18.73	0.12	20.32
2025-12-02T18:47:39.910	17.2d	UVOT	U	18.82	0.17	19.87
2025-12-02T18:51:29.880	17.2d	UVOT	UVW2	18.21	0.07	21.19
2025-12-02T18:57:56.170	17.2d	UVOT	UVM2	18.60	0.08	21.32
2025-12-05T13:27:51.135	19.9d	UVOT	UVW1	18.61	0.07	21.29
2025-12-05T13:30:04.874	19.9d	UVOT	U	18.75	0.10	20.55
2025-12-05T13:35:36.055	19.9d	UVOT	UVW2	18.38	0.05	22.23
2025-12-05T13:44:52.699	19.9d	UVOT	UVM2	18.61	0.06	22.26
2025-12-08T12:25:39.647	22.7d	UVOT	UVW1	18.98	0.13	20.39
2025-12-08T12:28:36.459	22.7d	UVOT	U	18.99	0.16	20.13
2025-12-08T12:34:31.294	22.7d	UVOT	UVW2	18.41	0.06	21.61
2025-12-08T12:44:51.692	22.7d	UVOT	UVM2	18.64	0.07	21.89
2025-12-11T04:14:36.004	25.2d	ZTF	g	19.58	0.18	19.97
2025-12-11T08:39:24.592	25.4d	UVOT	UVW1	18.81	0.08	21.21
2025-12-11T08:41:37.924	25.4d	UVOT	U	18.89	0.11	20.55
2025-12-11T08:47:09.915	25.4d	UVOT	UVW2	18.44	0.05	22.10
2025-12-11T08:56:31.579	25.4d	UVOT	UVM2	18.72	0.06	22.28
2025-12-12T03:23:56.003	26.2d	ZTF	g	19.53	0.14	20.23
2025-12-14T03:23:40.001	28.1d	ZTF	g	19.47	0.22	19.46
2025-12-14T04:29:12.998	28.1d	ZTF	r	19.89	0.18	19.89
2025-12-16T04:05:51.003	30.0d	ZTF	g	19.56	0.15	20.13
2025-12-16T05:37:21.999	30.1d	ZTF	r	20.07	0.23	19.84

2025-12-16T16:16:45.089	30.5d	UVOT	UVM2	18.85	0.07	21.40
2025-12-16T16:21:47.198	30.5d	UVOT	UVW1	18.95	0.08	21.49
2025-12-16T16:25:03.308	30.5d	UVOT	U	18.87	0.09	20.83
2025-12-16T16:27:33.770	30.5d	UVOT	UVW2	18.65	0.05	22.36
2025-12-18T03:07:40.996	31.9d	ZTF	r	20.09	0.22	19.70
2025-12-18T04:03:27.000	31.9d	ZTF	g	19.63	0.20	19.92
2025-12-18T07:35:41.441	32.0d	UVOT	UVM2	18.89	0.07	21.49
2025-12-18T07:41:49.428	32.0d	UVOT	UVW1	18.85	0.07	21.73
2025-12-18T07:45:40.330	32.0d	UVOT	U	18.90	0.08	20.98
2025-12-18T07:51:33.941	32.1d	UVOT	UVW2	18.58	0.05	22.50
2025-12-20T04:08:13.001	33.8d	ZTF	r	19.76	0.16	19.99
2025-12-20T10:33:34.136	34.1d	UVOT	UVM2	18.81	0.08	21.15
2025-12-20T10:40:48.033	34.1d	UVOT	UVW1	18.89	0.08	21.40
2025-12-20T10:45:09.833	34.1d	UVOT	U	19.07	0.11	20.74
2025-12-20T10:52:21.518	34.1d	UVOT	UVW2	18.68	0.06	22.27
2025-12-22T02:56:06.996	35.7d	ZTF	g	19.78	0.14	20.47
2025-12-22T03:03:17.001	35.7d	ZTF	r	20.15	0.18	20.42
2025-12-24T02:38:45.191	37.6d	UVOT	UVW1	18.98	0.11	20.77
2025-12-24T02:42:04.545	37.6d	UVOT	U	19.14	0.14	20.44
2025-12-24T02:49:50.256	37.6d	UVOT	UVW2	18.79	0.06	22.03
2025-12-24T02:59:44.831	37.6d	UVOT	UVM2	19.01	0.09	21.57

Table 2. Photometry of TDE 2025abcr. Phase is defined in rest-frame days relative to the lightcurve peak.

Date	Phase [days]	Instrument
2025-11-05T04:34:49.000	-9.0d	SEDm
2025-11-08T00:59:20.000	-6.3d	GHTS
2025-11-14T00:00:00.000	-0.6d	GHTS
2025-11-21T07:26:23.000	6.3d	LRIS
2025-11-26T06:15:50.000	11.0d	KAST
2025-11-30T01:12:46.000	14.6d	GHTS
2025-12-15T04:08:24.000	29.0d	LDT

Table 3. Spectroscopic observations of TDE 2025abcr. Phase is defined in rest-frame days relative to the lightcurve peak.

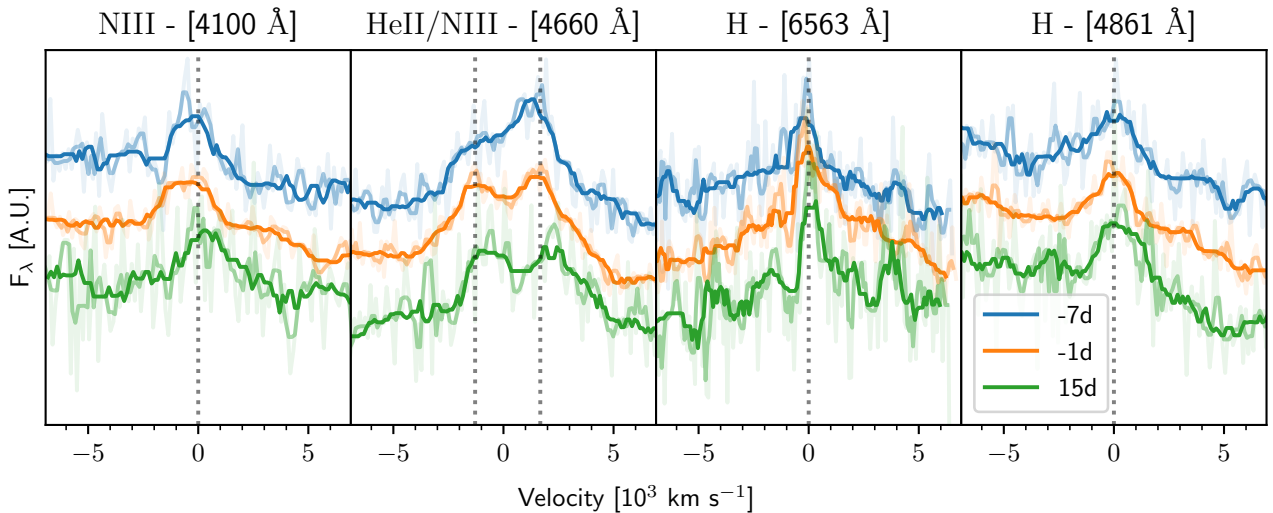


Figure 7. Zoomed-in velocity plots for an assortment of lines in the GHTS spectra of TDE 2025abcr, with times given in observer frame relative to the peak date and the central wavelength given in square brackets. The blended He II ($\lambda 4686$) / N III ($\lambda 4640$) feature evolves over time, with the N III becoming more prominent. Each of these lines is marked by a vertical dashed line.

UTC Start	UTC End	Phase [days]	Window [hr]	Luminosity [10^{41} erg s $^{-1}$]
2025-11-09T14:48:59.347	2025-11-09T14:57:20.807	-4.82	0.14	$39.4^{+17.7}_{-13.7}$
2025-11-09T16:31:25.310	2025-11-09T16:40:21.872	-4.75	0.15	$38.3^{+17.1}_{-13.2}$
2025-11-09T18:05:21.092	2025-11-09T23:01:17.524	-4.60	4.93	$13.7^{+5.6}_{-4.4}$
2025-11-14T05:13:41.900	2025-11-20T17:42:22.193	2.66	156.48	$2.9^{+1.9}_{-1.4}$
2025-11-23T14:56:16.906	2025-12-11T07:26:20.761	16.94	424.50	$1.5^{+1.1}_{-0.8}$
2025-12-11T10:04:27.529	2025-12-11T10:32:22.405	25.48	0.47	<6.9

Table 4. Dynamically-binned X-ray observations of TDE 2025abcr. Phase is defined in rest-frame days from the bin midpoint to the inferred peak time. We provide the unabsorbed 0.3-10 keV luminosity, as outlined in Section 3.6.

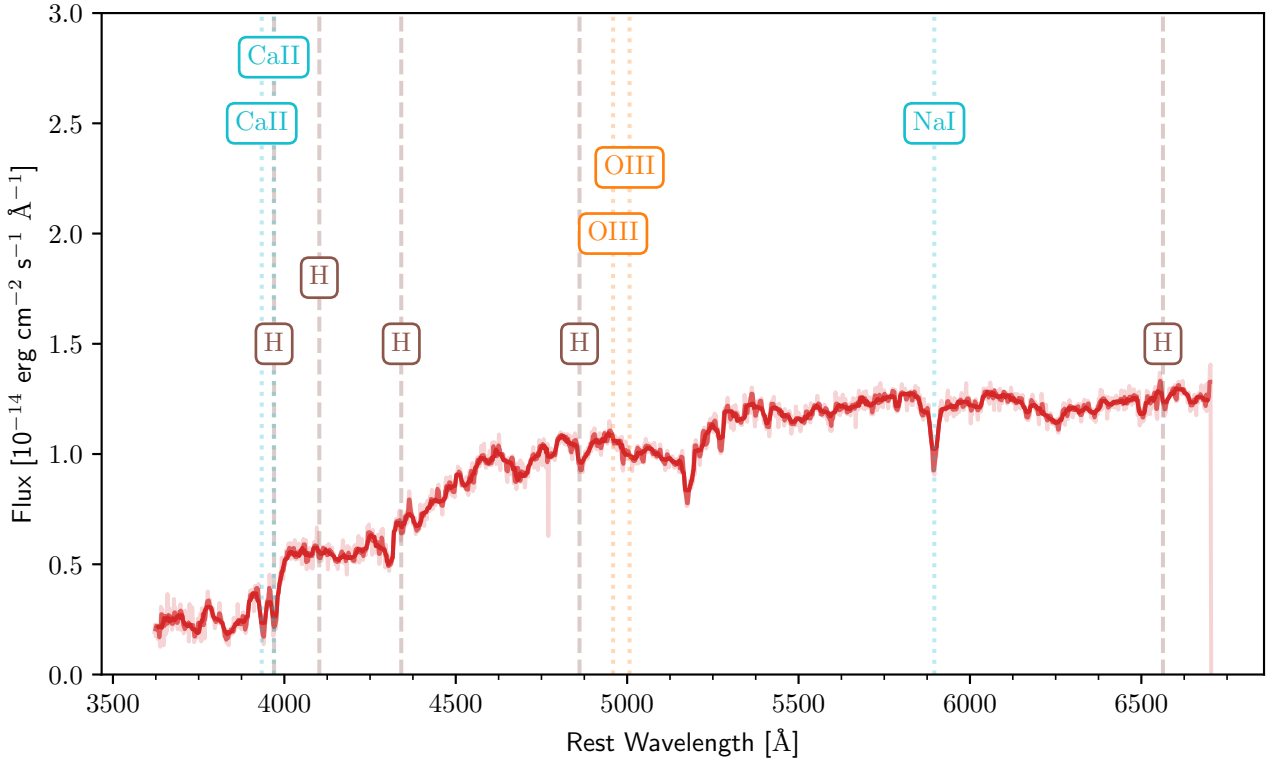


Figure 8. Spectrum of host WISEA J014656.04-152214.7, taken with GTHS. There is no evidence for typical AGN signatures (broad H or [O III]). However, clear absorption signatures are seen at Ca II and Na I, for a consistent redshift of $z = 0.0498$.

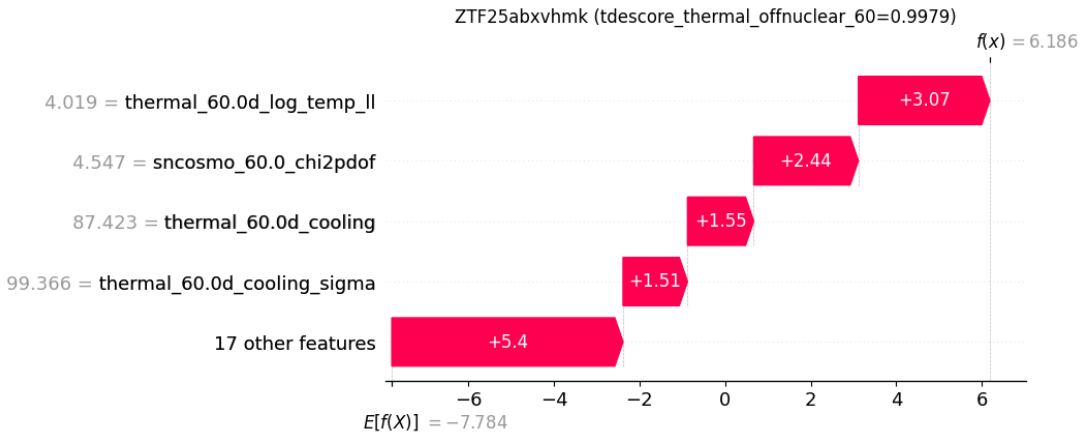


Figure 9. A waterfall plot highlights the main features which contribute to the ML classification of TDE 2025abcr as a likely TDE by `tdescore`, as described in R. Stein et al. (2024). As of 2025 November 29, the classification is driven primarily by the high lower bound on blackbody temperature ($T > 10^{4.02}$ K), the poor fit to a Type Ia SN with `sncosmo` (K. Barbary et al. 2016) (χ^2 per d.o.f. = 4.5), and the best-fit temperature increasing with time rather than cooling (+87 K per day). All properties are characteristic of TDEs (which are hot, slowly evolving and do not rapidly cool), but are not common for SNe (which have lower temperatures, more rapid evolution and generally cool more quickly). The exact parameters differ slightly from Section 4.1.1, because they are based on a fit to only ZTF data and include only photometry available up to 2025 November 29.

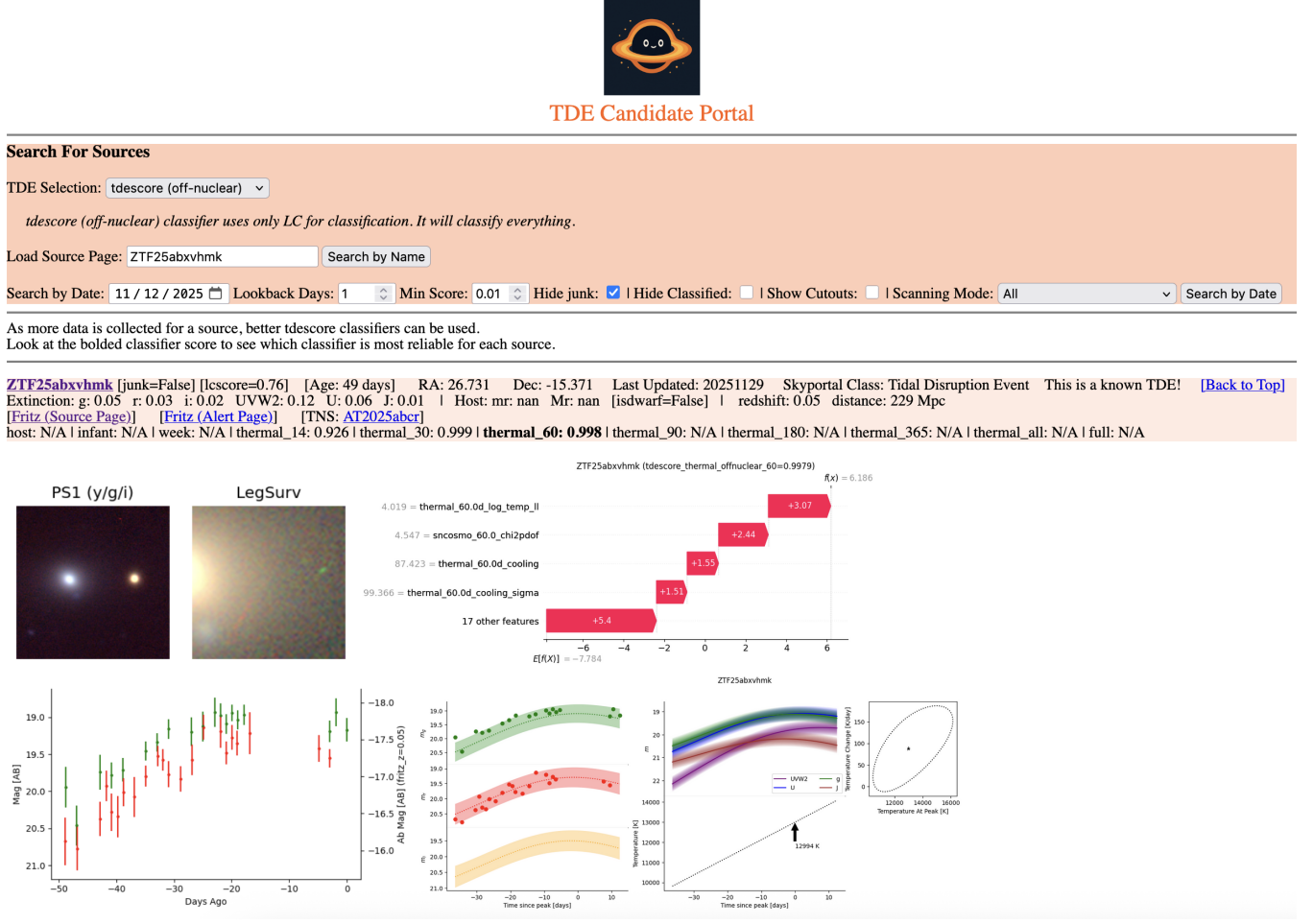


Figure 10. `tdescore` summary page for ZTF25abxvhmk / TDE 2025abcr as of 2025-11-29. The classifier relies on the lightcurve fit shown in the central lower panel, following the same blackbody procedure described in Section 4.1.1 and shown in the lower-right panel. The waterfall plot (center right) is reproduced in higher resolution in Figure 9.

Parameter	Best Fit	Lower Bound	Upper Bound	Prior	Unit
tau	$1.05^{+0.10}_{-0.13}$	0.1	10.0	Uniform	Gyr^{-1}
tage	$8.98^{+0.80}_{-1.07}$	0.1	10.1	Uniform	Gyr
dust2	$0.07^{+0.03}_{-0.03}$	0.0	1.0	Uniform	optical depth at 5500AA
logzsol	$0.19^{+0.01}_{-0.02}$	-1.8	0.2	Uniform	$\log(Z/Z_{\odot})$
log10(mass)	$11.39^{+0.02}_{-0.04}$	8.0	12.0	LogUniform	Solar masses formed
log10(surviving mass)	$11.18^{+0.02}_{-0.03}$	/	/	derived	Solar masses surviving

Table 5. Priors and best-fit values for the five parameters of the `prospector` fit. The surviving solar mass parameter is also shown, but this is a derived quantity that does not directly enter the fit.

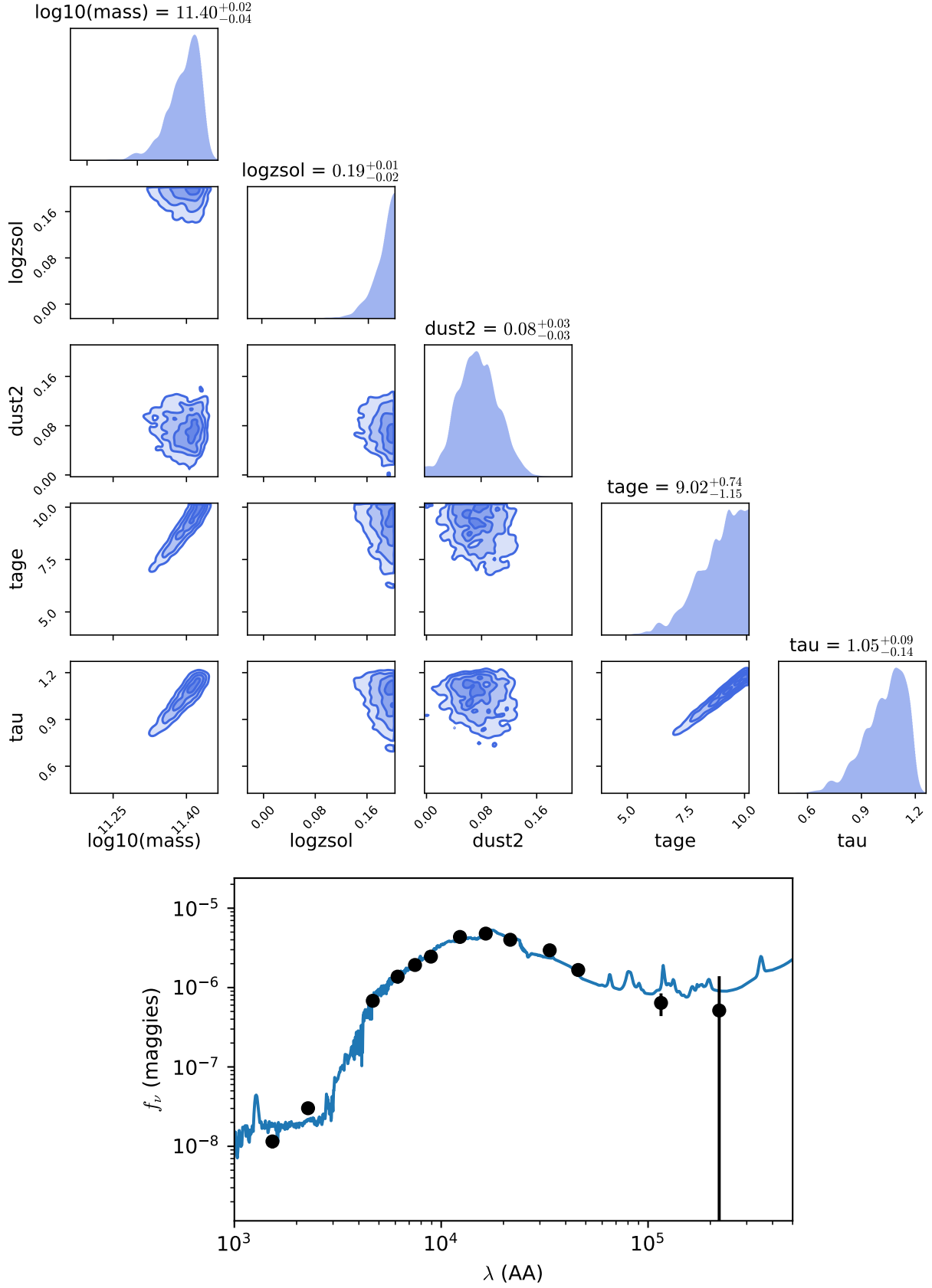


Figure 11. **Top:** Corner plot from the `prospector` fit, with the priors listed in Table 5. **Bottom:** Median SED (blue) and sampled uncertainty (orange) for the host galaxy, with measured photometry plotted in black. The `prospector` model provides a good fit to the data across the full wavelength range, from the UV to mid infra-red.

Name	z	Offset ("; kpc)	Parent M_{gal} (M_{\odot})	Satellite dwarf M_* (M_{\odot})	Central M_{BH} (M_{\odot})	TDE M_{BH} (M_{\odot})
3XMM J2150	0.05526	11.6; 12.5	$10^{10.93 \pm 0.07}$	$10^{7.3 \pm 0.4}$	$10^{8.49 \pm 0.67}$	$\sim 10^{4.9}$
EP240222a	0.03275	53.1; 34.7	$10^{10.89 \pm 0.07}$	$10^{7.0 \pm 0.3}$	$10^{8.44 \pm 0.67}$	$\sim 10^{4.9}$
TDE 2024tvd	0.04494	0.92; 0.81	$10^{10.93 \pm 0.02}$	$< 10^{7.6}$	$10^{8.37 \pm 0.51}$	$\sim 10^{5.9}$
TDE 2025abcr	0.04985	9.5; 10.3	$10^{11.18 \pm 0.03}$	$< 10^{7.4}$	$10^{8.82 \pm 0.65}$	$\sim 10^{6.1}$

Table 6. Summary of all off-nuclear TDEs, extended from the table of Y. Yao et al. (2025) with the inclusion of TDE 2025abcr.

REFERENCES

Amaro-Seoane, P., Audley, H., Babak, S., et al. 2017, arXiv e-prints, arXiv:1702.00786, doi: [10.48550/arXiv.1702.00786](https://doi.org/10.48550/arXiv.1702.00786)

Barbary, K., Barclay, T., Biswas, R., et al. 2016, SNCosmo: Python library for supernova cosmology,, *Astrophysics Source Code Library*, record ascl:1611.017 <http://ascl.net/1611.017>

Barth, A. J., Ho, L. C., & Sargent, W. L. W. 2002, *AJ*, 124, 2607, doi: [10.1086/343840](https://doi.org/10.1086/343840)

Begelman, M. C., Blandford, R. D., & Rees, M. J. 1980, *Nature*, 287, 307, doi: [10.1038/287307a0](https://doi.org/10.1038/287307a0)

Bellm, E. C., Kulkarni, S. R., Graham, M. J., et al. 2019, *PASP*, 131, 018002, doi: [10.1088/1538-3873/aaecbe](https://doi.org/10.1088/1538-3873/aaecbe)

Bertin, E. 2006, in *Astronomical Society of the Pacific Conference Series*, Vol. 351, *Astronomical Data Analysis Software and Systems XV*, ed. C. Gabriel, C. Arviset, D. Ponz, & S. Enrique, 112

Bertin, E., & Arnouts, S. 1996, *A&AS*, 117, 393, doi: [10.1051/aas:1996164](https://doi.org/10.1051/aas:1996164)

Bertin, E., Mellier, Y., Radovich, M., et al. 2002, in *Astronomical Society of the Pacific Conference Series*, Vol. 281, *Astronomical Data Analysis Software and Systems XI*, ed. D. A. Bohlender, D. Durand, & T. H. Handley, 228

Bhardwaj, K., Christov, A., & Karpov, S. 2025, *A&A*, 703, A95, doi: [10.1051/0004-6361/202556839](https://doi.org/10.1051/0004-6361/202556839)

Blagorodnova, N., Neill, J. D., Walters, R., et al. 2018, *PASP*, 130, 035003, doi: [10.1088/1538-3873/aaa53f](https://doi.org/10.1088/1538-3873/aaa53f)

Blecha, L., Sijacki, D., Kelley, L. Z., et al. 2016, *MNRAS*, 456, 961, doi: [10.1093/mnras/stv2646](https://doi.org/10.1093/mnras/stv2646)

Bricman, K., & Gomboc, A. 2020, *ApJ*, 890, 73, doi: [10.3847/1538-4357/ab6989](https://doi.org/10.3847/1538-4357/ab6989)

Burrows, D. N., Hill, J. E., Nosek, J. A., et al. 2005, *Space Sci. Rev.*, 120, 165, doi: [10.1007/s11214-005-5097-2](https://doi.org/10.1007/s11214-005-5097-2)

Busmann, M., O'Connor, B., Sommer, J., et al. 2025, arXiv e-prints, arXiv:2503.14588, doi: [10.48550/arXiv.2503.14588](https://doi.org/10.48550/arXiv.2503.14588)

Campanelli, M., Lousto, C., Zlochower, Y., & Merritt, D. 2007, *ApJ*, 659, L5, doi: [10.1086/516712](https://doi.org/10.1086/516712)

Cappellari, M. 2023, *MNRAS*, 526, 3273, doi: [10.1093/mnras/stad2597](https://doi.org/10.1093/mnras/stad2597)

Chambers, K. C., Magnier, E. A., Metcalfe, N., et al. 2016, arXiv e-prints, arXiv:1612.05560, doi: [10.48550/arXiv.1612.05560](https://doi.org/10.48550/arXiv.1612.05560)

Chang, Y.-C., Soria, R., Kong, A. K. H., et al. 2025, *ApJ*, 983, 109, doi: [10.3847/1538-4357/adbbee](https://doi.org/10.3847/1538-4357/adbbee)

Charalampopoulos, P. 2025a, *Transient Name Server Classification Report*, 2025-3466, 1

Charalampopoulos, P. 2025b, *Transient Name Server AstroNote*, 276, 1

Chen, J.-H., & Shen, R.-F. 2018, *ApJ*, 867, 20, doi: [10.3847/1538-4357/aadfd4](https://doi.org/10.3847/1538-4357/aadfd4)

Chornock, R., Hammerstein, E., Stein, R., & Carney, J. 2026a, *Transient Name Server Classification Report*, 2026-197, 1

Chornock, R., Hammerstein, E., Stein, R., & Carney, J. 2026b, *Transient Name Server AstroNote*, 7, 1

Chu, M., Dahiwale, A., & Fremling, C. 2021, *Transient Name Server Classification Report*, 2021-2672, 1

Clemens, J. C., Crain, J. A., & Anderson, R. 2004, in *Society of Photo-Optical Instrumentation Engineers (SPIE) Conference Series*, Vol. 5492, *Ground-based Instrumentation for Astronomy*, ed. A. F. M. Moorwood & M. Iye, 331–340, doi: [10.1117/12.550069](https://doi.org/10.1117/12.550069)

Coughlin, M. W., Bloom, J. S., Nir, G., et al. 2023, *ApJS*, 267, 31, doi: [10.3847/1538-4365/acdee1](https://doi.org/10.3847/1538-4365/acdee1)

Cross, N. J. G., Collins, R. S., Mann, R. G., et al. 2012, *A&A*, 548, A119, doi: [10.1051/0004-6361/201219505](https://doi.org/10.1051/0004-6361/201219505)

Dekany, R., Smith, R. M., Riddle, R., et al. 2020, *PASP*, 132, 038001, doi: [10.1088/1538-3873/ab4ca2](https://doi.org/10.1088/1538-3873/ab4ca2)

Dey, A., Schlegel, D. J., Lang, D., et al. 2019, *AJ*, 157, 168, doi: [10.3847/1538-3881/ab089d](https://doi.org/10.3847/1538-3881/ab089d)

Dgany, Y., Arcavi, I., Makrygianni, L., Pellegrino, C., & Howell, D. A. 2023, *ApJ*, 957, 57, doi: [10.3847/1538-4357/ace971](https://doi.org/10.3847/1538-4357/ace971)

Evans, P. A., Beardmore, A. P., Page, K. L., et al. 2009, *MNRAS*, 397, 1177, doi: [10.1111/j.1365-2966.2009.14913.x](https://doi.org/10.1111/j.1365-2966.2009.14913.x)

Faris, S., Arcavi, I., Newsome, M., et al. 2024, *Transient Name Server Classification Report*, 2024-4005, 1

Faris, S., Tranin, H., Newsome, M., & Arcavi, I. 2025, *Transient Name Server AstroNote*, 311, 1

Ferrarese, L., & Merritt, D. 2000, *ApJ*, 539, L9, doi: [10.1086/312838](https://doi.org/10.1086/312838)

Fitzpatrick, E. L. 1999, *PASP*, 111, 63, doi: [10.1086/316293](https://doi.org/10.1086/316293)

Foreman-Mackey, D., Hogg, D. W., Lang, D., & Goodman, J. 2013, *PASP*, 125, 306, doi: [10.1086/670067](https://doi.org/10.1086/670067)

Fragione, G., Leigh, N. W. C., Ginsburg, I., & Kocsis, B. 2018, *ApJ*, 867, 119, doi: [10.3847/1538-4357/aae486](https://doi.org/10.3847/1538-4357/aae486)

Franz, N., Alexander, K. D., Gomez, S., et al. 2025, arXiv e-prints, arXiv:2509.05405, doi: [10.48550/arXiv.2509.05405](https://doi.org/10.48550/arXiv.2509.05405)

Fremling, C., Miller, A. A., Sharma, Y., et al. 2020, *ApJ*, 895, 32, doi: [10.3847/1538-4357/ab8943](https://doi.org/10.3847/1538-4357/ab8943)

Gaia Collaboration. 2020, *VizieR Online Data Catalog*, I/350

Gaia Collaboration. 2021, *A&A*, 649, A1, doi: [10.1051/0004-6361/202039657](https://doi.org/10.1051/0004-6361/202039657)

Gebhardt, K., Bender, R., Bower, G., et al. 2000, *ApJ*, 539, L13, doi: [10.1086/312840](https://doi.org/10.1086/312840)

Gehrels, N. 1986, *ApJ*, 303, 336, doi: [10.1086/164079](https://doi.org/10.1086/164079)

Gehrels, N., Chincarini, G., Giommi, P., et al. 2004, *ApJ*, 611, 1005, doi: [10.1086/422091](https://doi.org/10.1086/422091)

Gezari, S. 2021, *ARA&A*, 59, 21, doi: [10.1146/annurev-astro-111720-030029](https://doi.org/10.1146/annurev-astro-111720-030029)

Gomez, S., Villar, V. A., Berger, E., et al. 2023, *ApJ*, 949, 113, doi: [10.3847/1538-4357/acc535](https://doi.org/10.3847/1538-4357/acc535)

Gössl, C. A., & Riffeser, A. 2002, *A&A*, 381, 1095, doi: [10.1051/0004-6361:20011522](https://doi.org/10.1051/0004-6361:20011522)

Graham, M. J., Kulkarni, S. R., Bellm, E. C., et al. 2019, *PASP*, 131, 078001, doi: [10.1088/1538-3873/ab006c](https://doi.org/10.1088/1538-3873/ab006c)

Greene, J. E., Strader, J., & Ho, L. C. 2020, *ARA&A*, 58, 257, doi: [10.1146/annurev-astro-032620-021835](https://doi.org/10.1146/annurev-astro-032620-021835)

Grotova, I., Rau, A., Baldini, P., et al. 2025, *A&A*, 697, A159, doi: [10.1051/0004-6361/202553669](https://doi.org/10.1051/0004-6361/202553669)

Guolo, M., Mummery, A., van Velzen, S., et al. 2025, arXiv e-prints, arXiv:2510.26774, doi: [10.48550/arXiv.2510.26774](https://doi.org/10.48550/arXiv.2510.26774)

Hammerstein, E., van Velzen, S., Gezari, S., et al. 2023, *ApJ*, 942, 9, doi: [10.3847/1538-4357/aca283](https://doi.org/10.3847/1538-4357/aca283)

HI4PI Collaboration, Ben Bekhti, N., Flöer, L., et al. 2016, *A&A*, 594, A116, doi: [10.1051/0004-6361/201629178](https://doi.org/10.1051/0004-6361/201629178)

Hoffman, L., & Loeb, A. 2007, *MNRAS*, 377, 957, doi: [10.1111/j.1365-2966.2007.11694.x](https://doi.org/10.1111/j.1365-2966.2007.11694.x)

Hopp, U., Bender, R., Grupp, F., et al. 2014, in Society of Photo-Optical Instrumentation Engineers (SPIE) Conference Series, Vol. 9145, Ground-based and Airborne Telescopes V, ed. L. M. Stepp, R. Gilmozzi, & H. J. Hall, 91452D, doi: [10.1111/12.2054498](https://doi.org/10.1111/12.2054498)

Hu, L., Wang, L., Chen, X., & Yang, J. 2022, *ApJ*, 936, 157, doi: [10.3847/1538-4357/ac7394](https://doi.org/10.3847/1538-4357/ac7394)

Hung, T., Gezari, S., Cenko, S. B., et al. 2018, *ApJS*, 238, 15, doi: [10.3847/1538-4365/aad8b1](https://doi.org/10.3847/1538-4365/aad8b1)

Ivezić, Ž., Kahn, S. M., Tyson, J. A., et al. 2019, *ApJ*, 873, 111, doi: [10.3847/1538-4357/ab042c](https://doi.org/10.3847/1538-4357/ab042c)

Jin, C. C., Li, D. Y., Jiang, N., et al. 2025, arXiv e-prints, arXiv:2501.09580, doi: [10.48550/arXiv.2501.09580](https://doi.org/10.48550/arXiv.2501.09580)

Johnson, B. D., Leja, J., Conroy, C., & Speagle, J. S. 2021, *ApJS*, 254, 22, doi: [10.3847/1538-4365/abef67](https://doi.org/10.3847/1538-4365/abef67)

Jones, D. H., Read, M. A., Saunders, W., et al. 2009, *MNRAS*, 399, 683, doi: [10.1111/j.1365-2966.2009.15338.x](https://doi.org/10.1111/j.1365-2966.2009.15338.x)

Kaiser, B. C., Clemens, J. C., Blouin, S., et al. 2021, *Science*, 371, 168, doi: [10.1126/science.abd1714](https://doi.org/10.1126/science.abd1714)

Karmen, M., Gezari, S., Norman, C., & Guolo, M. 2026, arXiv e-prints, arXiv:2602.04947. <https://arxiv.org/abs/2602.04947>

Khonji, N., Gualandris, A., Read, J. I., & Dehnen, W. 2025, *ApJ*, 994, 177, doi: [10.3847/1538-4357/ae0d8d](https://doi.org/10.3847/1538-4357/ae0d8d)

Kim, Y.-L., Rigault, M., Neill, J. D., et al. 2022, *PASP*, 134, 024505, doi: [10.1088/1538-3873/ac50a0](https://doi.org/10.1088/1538-3873/ac50a0)

Komossa, S., & Merritt, D. 2008, *ApJ*, 683, L21, doi: [10.1086/591420](https://doi.org/10.1086/591420)

Kormendy, J., & Ho, L. C. 2013, *ARA&A*, 51, 511, doi: [10.1146/annurev-astro-082708-101811](https://doi.org/10.1146/annurev-astro-082708-101811)

Lang-Bardl, F., Bender, R., Goessl, C., et al. 2016, in *Ground-based and Airborne Instrumentation for Astronomy VI*, Vol. 9908, SPIE, 1295–1302

Levine, S. E., Bida, T. A., Chylek, T., et al. 2012, in *Society of Photo-Optical Instrumentation Engineers (SPIE) Conference Series*, Vol. 8444, *Ground-based and Airborne Telescopes IV*, ed. L. M. Stepp, R. Gilmozzi, & H. J. Hall, 844419, doi: [10.1111/12.926415](https://doi.org/10.1111/12.926415)

Li, S., Berczik, P., Chen, X., et al. 2019, *ApJ*, 883, 132, doi: [10.3847/1538-4357/ab3e4a](https://doi.org/10.3847/1538-4357/ab3e4a)

Lin, D., Strader, J., Romanowsky, A. J., et al. 2020, *ApJ*, 892, L25, doi: [10.3847/2041-8213/ab745b](https://doi.org/10.3847/2041-8213/ab745b)

Lindgren, L., Klioner, S. A., Hernández, J., et al. 2021, *A&A*, 649, A2, doi: [10.1051/0004-6361/202039709](https://doi.org/10.1051/0004-6361/202039709)

Liu, F. K., & Chen, X. 2013, *ApJ*, 767, 18, doi: [10.1088/0004-637X/767/1/18](https://doi.org/10.1088/0004-637X/767/1/18)

Llamas Lanza, M., Karpov, S., Russeil, E., et al. 2025, arXiv e-prints, arXiv:2507.17499, doi: [10.48550/arXiv.2507.17499](https://doi.org/10.48550/arXiv.2507.17499)

Lomb, N. R. 1976, *Ap&SS*, 39, 447, doi: [10.1007/BF00648343](https://doi.org/10.1007/BF00648343)

Lützgendorf, N., Kissler-Patig, M., Neumayer, N., et al. 2013, *A&A*, 555, A26, doi: [10.1051/0004-6361/201321183](https://doi.org/10.1051/0004-6361/201321183)

Maksym, W. P., Ulmer, M. P., Eracleous, M. C., Guennou, L., & Ho, L. C. 2013, *MNRAS*, 435, 1904, doi: [10.1093/mnras/stt1379](https://doi.org/10.1093/mnras/stt1379)

Maksym, W. P., Ulmer, M. P., Roth, K. C., et al. 2014, *MNRAS*, 444, 866, doi: [10.1093/mnras/stu1485](https://doi.org/10.1093/mnras/stu1485)

Malyali, A., Rau, A., Bonnerot, C., et al. 2024, *MNRAS*, 531, 1256, doi: [10.1093/mnras/stae927](https://doi.org/10.1093/mnras/stae927)

Margutti, R., Zaninoni, E., Bernardini, M. G., et al. 2013, *MNRAS*, 428, 729, doi: [10.1093/mnras/sts066](https://doi.org/10.1093/mnras/sts066)

Martin, D. C., Fanson, J., Schiminovich, D., et al. 2005, *ApJ*, 619, L1, doi: [10.1086/426387](https://doi.org/10.1086/426387)

Martire, P., Rossi, E. M., Chamberlain Stone, N., et al. 2025, arXiv e-prints, arXiv:2512.10564, doi: [10.48550/arXiv.2512.10564](https://doi.org/10.48550/arXiv.2512.10564)

Masci, F. J., Laher, R. R., Rusholme, B., et al. 2019, *PASP*, 131, 018003, doi: [10.1088/1538-3873/aae8ac](https://doi.org/10.1088/1538-3873/aae8ac)

Masterson, M., De, K., Panagiotou, C., et al. 2024, *ApJ*, 961, 211, doi: [10.3847/1538-4357/ad18bb](https://doi.org/10.3847/1538-4357/ad18bb)

Melchior, P., Moolekamp, F., Jerdee, M., et al. 2018, *Astronomy and Computing*, 24, 129, doi: [10.1016/j.ascom.2018.07.001](https://doi.org/10.1016/j.ascom.2018.07.001)

Miller, J., & Stone, R. 1993, The Kast Double Spectrograph

Mo, G., Caiazzo, I., et al. in prep.,

Mockler, B., Melchor, D., Naoz, S., & Ramirez-Ruiz, E. 2023, *ApJ*, 959, 18, doi: [10.3847/1538-4357/ad0234](https://doi.org/10.3847/1538-4357/ad0234)

Mummery, A., van Velzen, S., Nathan, E., et al. 2024, *MNRAS*, 527, 2452, doi: [10.1093/mnras/stad3001](https://doi.org/10.1093/mnras/stad3001)

Neumayer, N., Seth, A., & Böker, T. 2020, *A&A Rev.*, 28, 4, doi: [10.1007/s00159-020-00125-0](https://doi.org/10.1007/s00159-020-00125-0)

Newsome, M., Faris, S., Arcavi, I., Dgany, Y., & Gomez, S. 2025, Transient Name Server Classification Report, 2025-4374, 1

Oke, J. B., Cohen, J. G., Carr, M., et al. 1995, *PASP*, 107, 375, doi: [10.1086/133562](https://doi.org/10.1086/133562)

Onken, C. A., Wolf, C., Bessell, M. S., et al. 2024, *PASA*, 41, e061, doi: [10.1017/pasa.2024.53](https://doi.org/10.1017/pasa.2024.53)

Pavez-Herrera, M., Sánchez-Sáez, P., Hernández-García, L., et al. 2025, *A&A*, 696, A153, doi: [10.1051/0004-6361/202451951](https://doi.org/10.1051/0004-6361/202451951)

Perley, D. A., Fremling, C., Sollerman, J., et al. 2020, *ApJ*, 904, 35, doi: [10.3847/1538-4357/abbd98](https://doi.org/10.3847/1538-4357/abbd98)

Prochaska, J. X., Hennawi, J. F., Westfall, K. B., et al. 2020a, arXiv e-prints, arXiv:2005.06505. <https://arxiv.org/abs/2005.06505>

Prochaska, J. X., Hennawi, J., Cooke, R., et al. 2020b, pypeit/PypeIt: Release 1.0.0, v1.0.0 Zenodo, doi: [10.5281/zenodo.3743493](https://doi.org/10.5281/zenodo.3743493)

Ramirez-Ruiz, E., & Rosswog, S. 2009, *ApJ*, 697, L77, doi: [10.1088/0004-637X/697/2/L77](https://doi.org/10.1088/0004-637X/697/2/L77)

Rees, M. J. 1988, *Nature*, 333, 523, doi: [10.1038/333523a0](https://doi.org/10.1038/333523a0)

Rejkuba, M. 2012, *Ap&SS*, 341, 195, doi: [10.1007/s10509-012-0986-9](https://doi.org/10.1007/s10509-012-0986-9)

Ricarte, A., Tremmel, M., Natarajan, P., & Quinn, T. 2021a, *ApJ*, 916, L18, doi: [10.3847/2041-8213/ac1170](https://doi.org/10.3847/2041-8213/ac1170)

Ricarte, A., Tremmel, M., Natarajan, P., Zimmer, C., & Quinn, T. 2021b, *MNRAS*, 503, 6098, doi: [10.1093/mnras/stab866](https://doi.org/10.1093/mnras/stab866)

Rigault, M., Neill, J. D., Blagorodnova, N., et al. 2019, *A&A*, 627, A115, doi: [10.1051/0004-6361/201935344](https://doi.org/10.1051/0004-6361/201935344)

Roming, P. W. A., Kennedy, T. E., Mason, K. O., et al. 2005, *Space Sci. Rev.*, 120, 95, doi: [10.1007/s11214-005-5095-4](https://doi.org/10.1007/s11214-005-5095-4)

Scargle, J. D. 1982, *ApJ*, 263, 835, doi: [10.1086/160554](https://doi.org/10.1086/160554)

Schlafly, E. F., & Finkbeiner, D. P. 2011, *ApJ*, 737, 103, doi: [10.1088/0004-637X/737/2/103](https://doi.org/10.1088/0004-637X/737/2/103)

Sfaradi, I., Margutti, R., Chornock, R., et al. 2025, *ApJ*, 992, L18, doi: [10.3847/2041-8213/ae0a26](https://doi.org/10.3847/2041-8213/ae0a26)

Sheng, X., Nicholl, M., Smith, K. W., et al. 2024, *MNRAS*, 531, 2474, doi: [10.1093/mnras/stae1253](https://doi.org/10.1093/mnras/stae1253)

Silverman, J. M., Foley, R. J., Filippenko, A. V., et al. 2012, *MNRAS*, 425, 1789, doi: [10.1111/j.1365-2966.2012.21270.x](https://doi.org/10.1111/j.1365-2966.2012.21270.x)

Skrutskie, M. F., Cutri, R. M., Stiening, R., et al. 2006, *AJ*, 131, 1163, doi: [10.1086/498708](https://doi.org/10.1086/498708)

Sollerman, J., Fremling, C., Perley, D., & Laz, T. D. 2024, Transient Name Server Discovery Report, 2024-3166, 1

Sollerman, J., Fremling, C., Perley, D., & Laz, T. D. 2025, Transient Name Server Discovery Report, 2025-4230, 1

Somalwar, J. J., Ravi, V., Dong, D. Z., et al. 2025a, *ApJ*, 982, 163, doi: [10.3847/1538-4357/adba4f](https://doi.org/10.3847/1538-4357/adba4f)

Somalwar, J. J., Ravi, V., Margutti, R., et al. 2025b, *ApJ*, 995, 228, doi: [10.3847/1538-4357/ae1501](https://doi.org/10.3847/1538-4357/ae1501)

Spergel, D. N. 2010, *ApJS*, 191, 58, doi: [10.1088/0067-0049/191/1/58](https://doi.org/10.1088/0067-0049/191/1/58)

Stein, R., van Velzen, S., Kowalski, M., et al. 2021, *Nature Astronomy*, 5, 510, doi: [10.1038/s41550-020-01295-8](https://doi.org/10.1038/s41550-020-01295-8)

Stein, R., Mahabal, A., Reusch, S., et al. 2024, *ApJ*, 965, L14, doi: [10.3847/2041-8213/ad3337](https://doi.org/10.3847/2041-8213/ad3337)

Stein, R., Carney, J., Andreoni, I., et al. 2025a, Transient Name Server Classification Report, 2025-4503, 1

Stein, R., Carney, J., Andreoni, I., et al. 2025b, Transient Name Server AstroNote, 317, 1

Stein, R., et al. in prep.,

Stein, R. D. 2025, robertdstein/galsynthspe: v0.2.1, v0.2.1 Zenodo, doi: [10.5281/zenodo.17634834](https://doi.org/10.5281/zenodo.17634834)

Stein, R. D., & Carney, J. 2025, robertdstein/uvotredux: v0.3.1, v0.3.1 Zenodo, doi: [10.5281/zenodo.17634569](https://doi.org/10.5281/zenodo.17634569)

Stein, R. D., Karambelkar, V., Kishore, S., et al. 2025, winter-telescope/mirar: v1.0.0 Release, v1.0.0 Zenodo, doi: [10.5281/zenodo.17592455](https://doi.org/10.5281/zenodo.17592455)

Steiner, J. F., Narayan, R., McClintock, J. E., & Ebisawa, K. 2009, *PASP*, 121, 1279, doi: [10.1086/648535](https://doi.org/10.1086/648535)

Stern, D., Assef, R. J., Benford, D. J., et al. 2012, *ApJ*, 753, 30, doi: [10.1088/0004-637X/753/1/30](https://doi.org/10.1088/0004-637X/753/1/30)

Stone, N., & Loeb, A. 2012, *MNRAS*, 422, 1933, doi: [10.1111/j.1365-2966.2012.20577.x](https://doi.org/10.1111/j.1365-2966.2012.20577.x)

Tang, V. L., Madau, P., Bortolas, E., et al. 2024, *ApJ*, 963, 146, doi: [10.3847/1538-4357/ad1dd9](https://doi.org/10.3847/1538-4357/ad1dd9)

Taylor, S. R. 2025, *Ap&SS*, 370, 124, doi: [10.1007/s10509-025-04513-9](https://doi.org/10.1007/s10509-025-04513-9)

Team, T. C., Bean, B., Bhatnagar, S., et al. 2022, *Publications of the Astronomical Society of the Pacific*, 134, 114501, doi: [10.1088/1538-3873/ac9642](https://doi.org/10.1088/1538-3873/ac9642)

van der Walt, S. J., Crellin-Quick, A., & Bloom, J. S. 2019, *Journal of Open Source Software*, 4, 1247, doi: [10.21105/joss.01247](https://doi.org/10.21105/joss.01247)

van Velzen, S., Stone, N. C., Metzger, B. D., et al. 2019, *ApJ*, 878, 82, doi: [10.3847/1538-4357/ab1844](https://doi.org/10.3847/1538-4357/ab1844)

van Velzen, S., Farrar, G. R., Gezari, S., et al. 2011, *ApJ*, 741, 73, doi: [10.1088/0004-637X/741/2/73](https://doi.org/10.1088/0004-637X/741/2/73)

van Velzen, S., Gezari, S., Hammerstein, E., et al. 2021, *ApJ*, 908, 4, doi: [10.3847/1538-4357/abc258](https://doi.org/10.3847/1538-4357/abc258)

Vazdekis, A., Koleva, M., Ricciardelli, E., Röck, B., & Falcón-Barroso, J. 2016, *MNRAS*, 463, 3409, doi: [10.1093/mnras/stw2231](https://doi.org/10.1093/mnras/stw2231)

Virtanen, P., Gommers, R., Oliphant, T. E., et al. 2020, *Nature Methods*, 17, 261, doi: [10.1038/s41592-019-0686-2](https://doi.org/10.1038/s41592-019-0686-2)

Wang, L., Höflich, P., & Wheeler, J. C. 1997, *ApJ*, 483, L29, doi: [10.1086/310737](https://doi.org/10.1086/310737)

Wright, E. L., Eisenhardt, P. R. M., Mainzer, A. K., et al. 2010, *AJ*, 140, 1868, doi: [10.1088/0004-6256/140/6/1868](https://doi.org/10.1088/0004-6256/140/6/1868)

Yao, Y., Ravi, V., Gezari, S., et al. 2023, *ApJ*, 955, L6, doi: [10.3847/2041-8213/acf216](https://doi.org/10.3847/2041-8213/acf216)

Yao, Y., Chornock, R., Ward, C., et al. 2025, *ApJ*, 985, L48, doi: [10.3847/2041-8213/add7de](https://doi.org/10.3847/2041-8213/add7de)

York, D. G., Adelman, J., Anderson, John E., J., et al. 2000, *AJ*, 120, 1579, doi: [10.1086/301513](https://doi.org/10.1086/301513)

Yuan, W., Zhang, C., Chen, Y., & Ling, Z. 2022, in *Handbook of X-ray and Gamma-ray Astrophysics*, ed. C. Bambi & A. Sanganello, 86, doi: [10.1007/978-981-16-4544-0_151-1](https://doi.org/10.1007/978-981-16-4544-0_151-1)

Zhang, Z., Yao, Y., Gilfanov, M., et al. 2025, arXiv e-prints, arXiv:2512.12480, doi: [10.48550/arXiv.2512.12480](https://doi.org/10.48550/arXiv.2512.12480)

Zheng, R., Lin, Z., Kong, X., et al. 2025, arXiv e-prints, arXiv:2512.24782, doi: [10.48550/arXiv.2512.24782](https://doi.org/10.48550/arXiv.2512.24782)